


Secretins of type-two secretion systems are necessary for exopolymeric slime secretion in cyanobacteria and myxobacteria

Received: 29 April 2022

David M. Zuckerman^{1,3}, Jeffery Man To So^{2,3} & Egbert Hoiczky²✉

Accepted: 18 August 2025

Published online: 26 September 2025

 Check for updates

Cyanobacteria and myxobacteria display gliding motility associated with the secretion of an exopolymeric slime through nozzle-like structures. Here, we use biochemical and structural assays to show that these nozzles are composed of secretins of the PilQ/GspD family, which are known to form outer membrane gates in type-two secretion systems (T2SSs) and other bacterial protein secretion systems. We show that *gspD* is an essential gene in *Myxococcus xanthus*, and its downregulation by conditional knockdown renders this bacterium defective in both slime secretion and gliding motility. In cyanobacteria, available data suggest that the exopolymeric slime is a polysaccharide, although the precise nature of the slime in myxobacteria remains unclear. Our results, therefore, indicate that secretins may be required for the secretion of non-proteinaceous polymers in certain bacteria.

Secretion of macromolecules is an important component of environmental adaptation, and a key property of any living cell. Like eukaryotic cells, bacteria contain dedicated macromolecular secretion systems in the cell envelope that are used to translocate proteins, nucleic acids, and carbohydrates¹. Despite an extraordinary diversity of both substrates and bacterial cell physiologies, there are only a limited number of secretion systems. In Gram-negative bacteria, eleven protein (type I–XI^{1–5}), one nucleic acid (type IV⁶), and three carbohydrates (Wzx/Wzy, ABC transporter, and synthase-dependent⁷) secretion systems have been described. Moreover, a close inspection of these molecular machines reveals the utilization of multiple homologous proteins, suggesting divergence from common ancestry. Diversity between the systems appears to have evolved through use of novel proteins, and matching of protein components between translocation machineries⁸.

One well-studied component of secretory machinery shared between several systems is the secretin family of proteins^{9–11}. These multimeric proteins form the outer membrane (OM) gates of the type II and III secretion systems, the type IV pilus apparatus, and filamentous phage extrusion machinery^{12–14}. Secretins form a functional channel with an OM pore that is 5–8 nm wide, allowing the passage of large cargo molecules such as folded proteins and multimeric protein fibers. These channels are typically formed by the assembly of 15

monomers of GspD (e.g., GspD_{Ecol} 15mer PDB ID code 5WQ7), or 12 to 14 (in some cases up to 19¹⁵) monomers of PilQ (e.g., PilQ_{Mxan} 12mer PDB ID code 3JC9; PilQ_{Paer} 14mer PDB ID code 6VE3^{10,16–18}). Nearly all secretins (with the known exception of HxcQ of *Pseudomonas aeruginosa*¹⁹) require additional proteins, called pilotins or accessory proteins, for their assembly. These proteins contribute to stability, OM targeting, and oligomerization of the secretins²⁰. Secretins can be identified by highly-conserved C-terminal secretin domains that form the OM-embedded portion of the complex^{21,22}. In contrast, the N-terminal domains exhibit greater sequence variability and assemble into multiple ring structures that form a large periplasmic vestibule^{21,23}. These domains also create a prominent constriction called the periplasmic gate, which is positioned between the vestibule and the secretin chamber. The secretin chamber itself contains a second constriction at its midpoint, known as the secretin gate. Based on leaky phenotypes of secretin gate mutant strains, this structure appears to restrict the size of the secretin pore to that of typical porins, preserving the outer membrane's barrier function^{22–25}. The periplasmic gate, in contrast, likely facilitates the alignment and entry of cargo into the secretin chamber. The N-terminal periplasmic domains also interact with the components of the cytoplasmic membrane-embedded platform of the secretion machinery, to promote channel opening, cargo docking, and subsequent release^{26,27}. Importantly, this process must be

¹Biology Department, Iona University, New Rochelle, NY, USA. ²School of Biosciences, Krebs Institute, University of Sheffield, Sheffield, UK. ³These authors contributed equally: David M. Zuckerman, Jeffery Man To So. ✉e-mail: egbert.hoiczky@gmail.com

highly controlled to prevent unintended breaches of the OM. Although the cargos of the best-understood systems are folded proteins or protein fibers, the transient interactions with the channel should theoretically enable secretins to translocate highly diverse molecules, including non-proteinaceous ones.

While protein secretion has long been studied in Gram-negative bacteria, our understanding of the secretion of additional extracellular materials is less complete^{28–30}. In part, this is because the complexity of extracellular polymeric substances (EPS) is confounding. For example, many EPS species are composed of polysaccharides³¹, and bacteria utilize a greater diversity of monosaccharides than amino acids. These monosaccharides are connected by various chemical linkages, and are further diversified by chemical alterations introduced by enzymatic modification (for example see refs. 32,33). Despite these differences, the secretion of both protein and EPS poses similar challenges to the cell, as bulky, hydrophilic, high-molecular-weight polymers are translocated across hydrophobic membranes. So far, three different mechanisms have been described for EPS secretion in Gram-negative bacteria³⁰, for a review in *Myxococcus xanthus* see³⁴): the Wzx/Wzy, the ABC transporter, and the synthase-dependent secretion pathways. The Wzx/Wzy pathway is used by bacteria for the synthesis of group I capsular exopolysaccharide, O-antigen lipopolysaccharide (LPS), and succinoglycan EPS, which are synthesized from sugar phosphates that bind to a carrier lipid in the cytoplasmic membrane^{28–30}. Upon binding, the monomers form short oligosaccharides that are flipped across the membrane, polymerized by a periplasmic enzyme (Wzy), and fed into the Wza channel³⁵. The ABC transporter pathway is used for group 2 capsular polysaccharides, the LPS common antigens, and N-glycosylation of outer membrane and periplasmic proteins, in which the entire carbohydrate is synthesized on a carrier lipid before being transported across the cytoplasmic membrane via an ABC transporter^{30,36}. Both the Wzx/Wzy and the ABC transporter pathways rely on proteins of the polysaccharide co-polymerase (PCP) and OM polysaccharide export (OPX) protein families for OM translocation^{37–39}. Although members of the OPX protein families can be easily identified using bioinformatics, structural data for their proteins are scarce. The only exception is the Wza channel (PDB ID code 2J58) of the Wzx/Wzy system from *E. coli*, which has been resolved at atomic resolution⁴⁰. Of note, the tandem β -grasp fold that forms the periplasmic domain of Wza can also be found in the group 4 polysaccharide capsule protein GfC⁴¹. However, the exact role of GfC in polymer secretion is yet to be determined⁴². For the PCP protein family, full-length structures of Class 1 PCP Wzz (PDB ID code 6RBG) and Class 2 PCP Wzc (PDB ID code 7NHR) have recently been solved using cryo-electron microscopy^{43,44}. The third EPS secretion mechanism, which appears to be used by bacteria for the secretion of many high-molecular-weight polysaccharide moieties, such as cellulose⁴⁵, alginate⁴⁶, and poly- β -D-N-acetylglucosamine (PNAG⁴⁷), is called the synthase-dependent pathway⁷, referring to the fact that a cytoplasmic membrane-embedded glycosyl transferase simultaneously facilitates polymerization and trans-membrane translocation⁴⁸. Depending on the substrate in question, these steps can be performed with or without participation of a carrier lipid and, in some cases, are stimulated by the bacterial second messenger bis-(3'-5')-cyclic dimeric guanosine monophosphate (c-di-GMP⁴⁹). Once in the periplasm, the newly formed polymer interacts with a tetratricopeptide repeat (TPR-) containing protein⁵⁰ and is released through an OM porin like AlgE⁵¹ (PDB ID code 3RBH).

While some EPS polymers with relevance to medicine and industry have been widely studied²⁹, the majority of EPS molecules produced by environmental bacteria are poorly characterized. One such environmental EPS, often referred to as slime, is deposited as trails behind certain gliding bacteria⁵², including cyanobacteria⁵³ and myxobacteria⁵⁴. Although it is generally believed that slime is composed of carbohydrates, this has been experimentally verified in a few cases, for example, the filamentous cyanobacterium

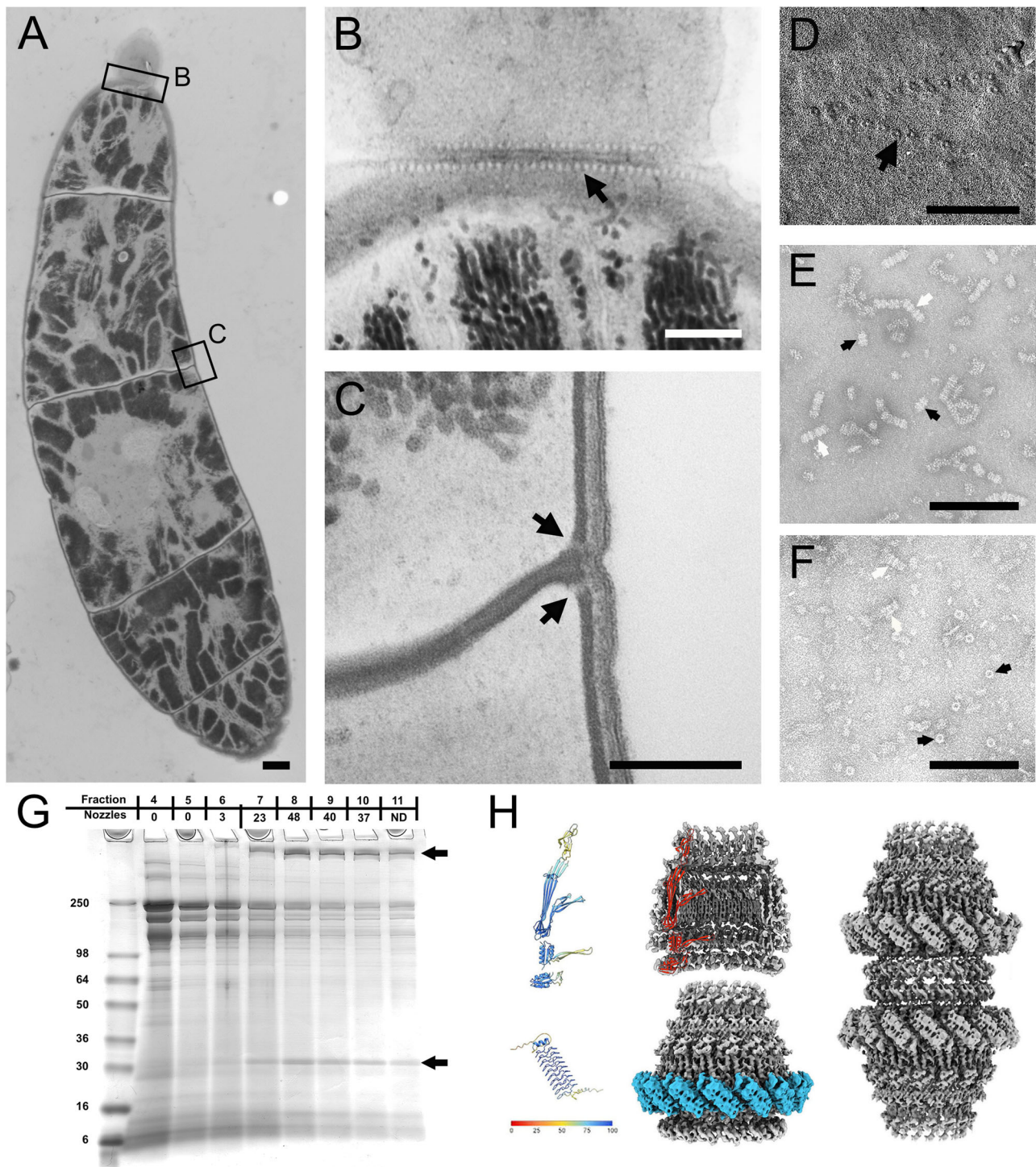
Phormidium uncinatum; in this species, the EPS slime is composed of six monosaccharides, with glucose (34%) and xylose (33%) being the most abundant⁵⁵. The composition of slime in myxobacteria has not been experimentally determined. Despite reports of *M. xanthus* slime trails having been stained with the lectin concanavalin A⁵⁶, this species has also been described to secrete a calcofluor white-stainable carbohydrate termed EPS that is important for type IV pilus motility⁵⁷, and is unambiguously not slime. For specificity, we refer to the material forming the slime trails as AEP (A-motility-related exopolymer). Despite this lack of chemical characterization, it is generally accepted that slime secretion in these organisms is important for motility⁵⁸, the precise contribution in some gliding microbes is less clear⁵⁶ due to the absence of information on the characteristics of slime. Namely, the composition of the slime, enzymes that synthesize the slime, and the slime secretion apparatus have yet to be determined.

In this study, we use structural and biochemical assays to identify the OM secretion channel for slime. We found that the secretins PilQ and GspD constitute the slime-secretion nozzles in cyanobacteria and myxobacteria, respectively. Our results show for the first time that secretins can facilitate the translocation of molecules other than proteins or protein fibers, considerably expanding the repertoire of substrates of these multifunctional OM gates. Moreover, our results show that *gspD* is an essential gene in *M. xanthus* that, when depleted, renders this bacterium defective in APS slime secretion and motility, confirming that GspD-facilitated secretion is essential for gliding in this bacterium. Here we show that secretins, in addition to contributing to protein secretion and pilus-mediated host attachment, also contribute to motility and biofilm formation.

Results

PilQ forms the slime nozzle in filamentous cyanobacteria

Previously, we demonstrated that cyanobacteria of the genera *Oscillatoria*, *Phormidium*, *Lyngbya*, and *Anabaena* used rows of tilted nozzles (junctional pore complexes) at the cross walls of their multicellular filaments to secrete bands of slime^{53,59} (Fig. S1). Since these bands elongated at the same rate with which the filaments were moving, it was proposed that slime secretion powers gliding motility⁶⁰. We wished to identify the slime secretion apparatus; however, the complex culture requirements of these species made isolating these nozzles impossible at the time⁶¹. Therefore, we initially used the more easily cultivated species *Arthrospira* (*Spirulina*) *platensis* for the current study⁶². As this free-floating species is usually cultivated in aerated reactor vessels, most available clones are non- or temporarily non-motile. For that reason, we initially confirmed that our clone secreted slime using direct observations⁵³ and was able to glide in an established clumping assay (refs. 63,64; Fig. S2). Next, thin sections of cryo-substituted cells were analyzed by electron microscopy to confirm the presence of the tilted trans-peptidoglycan channels harboring the nozzle apparatus (Fig. 1A–C). Rotary shadowing and negative staining of preparations of isolated OMs were used to directly visualize rows of nozzles (Fig. 1D). Together, these results documented that the cell envelope architecture and arrangement of nozzles in *A. platensis* is identical to all of our previously studied filamentous cyanobacteria⁵⁹. To identify the major component(s) of the nozzles, we next purified cell envelopes, fractionated, and screened for the presence of nozzle-like complexes using electron microscopy. This strategy yielded nozzle-enriched fractions, devoid of any other large complexes (Fig. 1E). Ring-shaped top views of the complexes were also observed upon adsorption to grids without glow discharge, likely due to a preferential adsorption of the complex on these grids (Fig. 1F), as previously reported⁵³. These nozzle-enriched fractions were separated by SDS-PAGE, and revealed two prominent protein bands at >250 and 30 kDa (Fig. 1G). Mass spectrometry and Edman degradation identified these proteins as the secretin PilQ (Table S2) and the pentapeptide



repeat protein NIES39_A07680⁶⁵. We noted that the calculated molecular weight of PilQ is ca. 80 kDa, but identified PilQ from a band that migrated much more slowly, and in only modest amounts from highly enriched fractions (Fig. 1E vs. G). Paradoxically, increasing the nozzle concentration resulted in a decline of the 250 kDa band, whereas at low concentrations, PilQ runs at ca. 98 kDa which is closer to its calculated molecular weight. Increasing the nozzle concentration causes a shift and eventual disappearance of this initial band and the appearance of the ca. 250 kDa band, similar to our observations from purified nozzle structures (Fig. S3). As the PilQ concentration is further increased, the signal disappears altogether, likely due to the formation of increasingly larger aggregates of PilQ that fail to enter the gel.

To further confirm that PilQ forms the nozzles complexes, we initially attempted immunogold labeling for electron microscopy, using the cross-reacting antiserum raised against GspD from *M. xanthus* (Fig. S4A). Unfortunately, due to the low number of nozzles among the isolated protein complexes the on-grid labeling results were unsatisfactory. Consequently, we opted for an integrative cryo-EM AlphaFold-based reconstruction of ice-embedded nozzles, using the two identified proteins, PilQ and NIES39_A07680, as templates (Fig. 1H; Figs. S5–6; Table S1). Due to the limited number of available particles, achieving a high-resolution reconstruction was not possible. However, at >4 Å resolution, the structures of the two proteins obtained from the AlphaFold Protein Structure Database^{66,67} fit well

Fig. 1 | PilQ forms the slime nozzle in filamentous cyanobacteria. A–C Thin sections of high-pressure frozen *Athospora platensis* cells show the tilted trans-peptidoglycan channels harboring the nozzle apparatus (black arrows), which are arranged in a circumferential ring at each cross wall. **B, C** High magnification micrographs from the indicated regions in (A). To best visualize more channels, **B** shows an image selected from the thin section series of the area shown in (A). The black arrows indicate the position of the transpeptidoglycan channels that in cross sections are visible as small white dots (**B**) and in longitudinal sections as slightly angled less dark-stained bands traversing the peptidoglycan at an angle of 30–40° relative to the septum (**C**). Shown are representative images of a cell filament from two separate experiments, each involving over a hundred thin-sectioned filaments. **D** Platinum-carbon (Pt/C) shadowing of an isolated outer membrane patch reveals the rows of nozzles (black arrow) consisting of the peripheral ring (16–18 nm) and a central pore (6–8 nm) which have identical dimensions as the top views of the isolated pores (black arrows) in (F). The data presented are from a single experiment and have been validated by additional findings from negative staining (F). **E** Transmission electron microscope image of a negatively stained isolated nozzle preparation. Black arrows indicate individual double ring nozzles, while white arrows indicate linear arrays containing multiple nozzles. The length of an individual double nozzle is ca. 32 nm. **F** As has been observed for nozzles of other filamentous cyanobacteria, adsorption to grids without glow discharge reveals top views of the complex (black arrows), while only a few side views are visible (white arrows) demonstrating that the cyanobacterial and myxobacterial nozzles (Fig. 3C) share similar architecture. The image in (E) represents data from at least 200

independent isolation experiments, whereas **F** shows a representative image from five independent experiments. **G** Fractions from a slime nozzle enrichment were screened by TEM and scored for how many nozzles were observed per grid square (ND, not determined). Fractions were separated by SDS-PAGE, and two bands correlated with fractions enriched for nozzles, identified as PilQ (black arrow, higher MW band), and the pentapeptide repeat protein NIES39_A07680 (black arrow, lower MW band). Size markers (first lane) indicate molecular weight in kDa. The image shows a representative SDS-PAGE gel from ten independent experiments. **H** Integrative cryo-EM and AlphaFold 3D reconstruction of the isolated PilQ nozzle complexes. The ribbon diagrams on the left show AlphaFold's structure predictions for PilQ (upper drawing) and NIES39_A07680 (lower drawing). The color bar below represents the per-residue % confidence metrics (predicted local distance difference test, pLDDT) of the two structures, with blue indicating high confidence. The PilQ reconstruction is segmented into domains but lacks the NO domain (amino acid residues 1–240), which could not be matched with the electron density. The middle and right structures present various views of the integrative cryo-EM reconstruction and AlphaFold prediction of PilQ: A vertical cross-section through the PilQ-only reconstruction highlights a single PilQ monomer in red (middle top). The 3D reconstruction depicts the 16mer PilQ ring-shaped oligomer with attached NIES39_A07680 monomers in blue (middle bottom) and has a resolution of approximately 4 Å (Fig. S5). Lastly, a 3D reconstruction of the isolated double particles is shown, which strikingly resembles the nozzles previously isolated from *Ph. uncinatum* (see Fig. S7³³). Scale bars: **A** 1 µm; **B** 250 nm; **C–F** 200 nm. Source data are provided as a Source Data file.

into the cryo-EM-resolved structure. PilQ, exhibiting 16-fold rotational symmetry, forms the cylindrical main body of the complex, while the compact solenoid structure of NIES39_A07680 accounts for most of the massive lower ring of the structure, distinguishing it from other secretin complexes. This interpretation is further supported when negatively stained *A. platensis* nozzle complexes are compared with published averages of other secretin complexes. The structural similarities, even with distantly related complexes, further strengthen our interpretation that PilQ forms the nozzles of filamentous cyanobacteria (Fig. S7).

With a candidate nozzle protein identified, we next attempted to visualize PilQ at the sites of slime secretion in situ. Although the ease of cultivation of *A. platensis* initially offered advantages, with continuous culture a substantial portion of the filaments lost their PilQ nozzles, ceased secreting slime, and became non-motile, a phenomenon that we had previously observed in permanently agitated cultures of benthic gliding cyanobacteria⁶⁸. As this mixed population of nozzle-containing and nozzle-free filaments yielded inconsistent results, we decided to use two highly motile benthic species, *Oscillatoria lutea* (UTEX 1814) and *Phormidium autumnale* (ATFG6) for further experiments. Genome sequence was obtained from both strains, and the gene for *pilQ* from *O. lutea* was expressed in *E. coli*. Protein was purified and used to inoculate rabbits to raise antisera. Although this antibody specifically cross-reacted with the PilQ band of both species in immunoblots (Fig. S4B), initial attempts at fluorescent labeling of the nozzles in live filaments were unsuccessful. We attributed these difficulties to the inaccessibility of PilQ epitopes due to the complex multilayered architecture of cyanobacterial cell envelopes. Here, the PilQ-containing outer membrane is sandwiched between a many-nanometer-thick and heavily cross-linked peptidoglycan layer and an extracellular barrier comprised of an S-layer topped by the helically arranged glycoprotein oscillin^{59,68,69}; Fig. S1). To potentially increase access for the antibodies, we used isolated cell envelopes for our labeling experiments, but again failed to observe labeling of the PilQ nozzles at cell-cell junctions. However, within these preparations, we consistently observed isolated disc-shaped cross walls that still had the nozzle-containing portion of the longitudinal wall attached (observed by the pores in the cell wall), and we saw clear peripheral immunolabeling of these cross walls with the anti-PilQ antisera (Fig. 2A, B; Fig. S8). These results supported our initial interpretation that PilQ epitopes were masked in our earlier attempts to immunolabel intact

cells. Since a number of conventional permeabilization methods, such as lysozyme or organic solvent treatment, failed to allow labeling or resulted in the disintegration of the filaments, we attempted to perform limited cell lysis to remove some of the cell wall material. Exposure of live filaments to high or low temperatures (50 °C or 4 °C) or incubation with 200 mM DTT⁷⁰ were among the most reproducible treatments to induce limited cell lysis. Upon treatment of the filaments, the rows of nozzles were clearly labeled with the anti-PilQ antibody, confirming that the nozzles at the cross walls were indeed composed of PilQ (Fig. 2C). In contrast, pre-immune sera controls failed to label the nozzles (Fig. S9). Unfortunately, the extensive multi-step treatment required for immunofluorescence imaging of the nozzles precluded the possibility to simultaneously retain and visualize slime secretion. Consequently, we used fluorescently-labeled concanavalin A to visualize slime secretion in living cells to determine whether slime trails emerged from the cross walls, where nozzles are located. As the fluorescently labeled slime bands usually translocate along the filaments' surfaces (Fig. 2D), we had to apply a continuous flow to shear them from the surface. Under these conditions, the slime detached from the filament surface⁵³, revealing individual strands. However, the high gliding speed of these cells and the copious amount of slime secreted posed additional challenges in locating the precise origin of secretion (Fig. 2E). Subjecting the cell filaments to a gentle burst of sonication and cooling before imaging appeared to encourage slime detachment and decrease gliding speed, respectively. With these treatments, we observed individual strands of slime emanating in close proximity to mature and nascent cross walls (Fig. 2F), where PilQ nozzles are located (Fig. 2A, B; Fig. S1). This is consistent with a previous report of the localization of slime secretion when slime was stained using India Ink⁵³. Moreover, the fact that the lectin concanavalin A specifically stains the secreted EPS slime of *O. lutea* supports previous chemical analysis of *P. uncinatum* EPS slime⁵⁵ and strongly supports the idea that the EPS slime in cyanobacteria is a carbohydrate. Taken together, this evidence supports the interpretation that the secretin PilQ is used for EPS carbohydrate slime secretion in filamentous cyanobacteria.

GspD is a candidate for slime nozzles in *M. xanthus*

Because multicellular filamentous cyanobacteria are difficult to genetically manipulate, and to test if other slime-secreting bacteria also use secretin nozzles, we next studied the soil bacterium *M.*

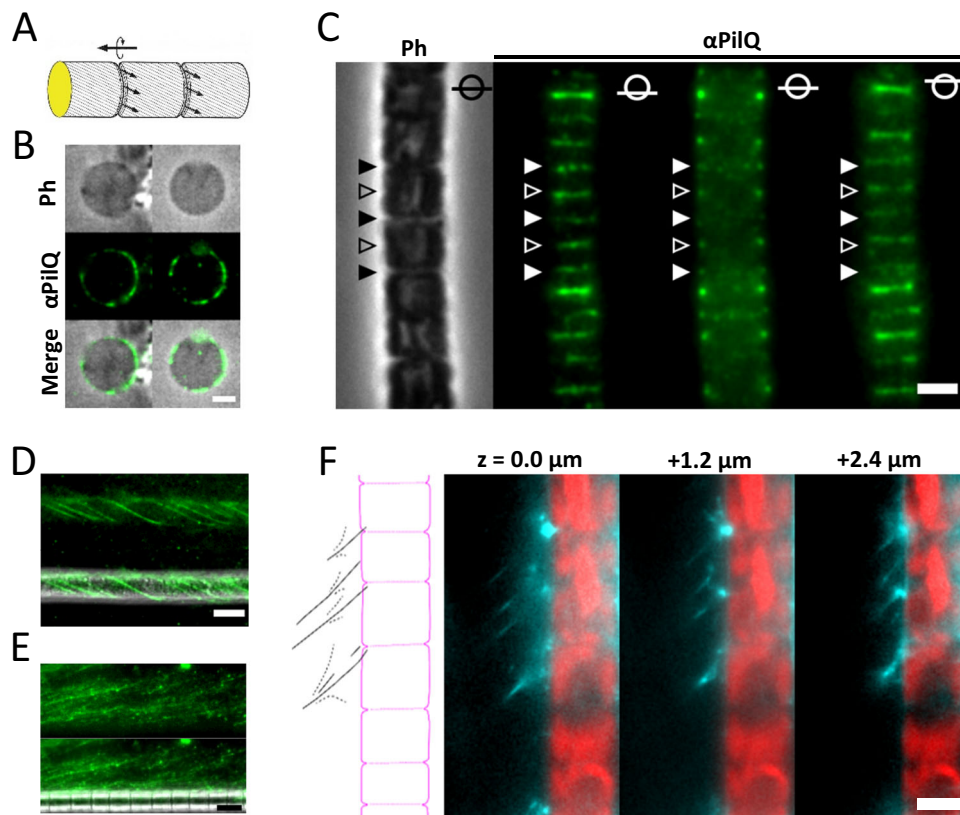


Fig. 2 | Immunofluorescence microscopy of *Oscillatoria lutea* and *Phormidium autumnale* filaments showing the localization of PilQ at the cross walls where EPS is secreted. **A** Schematic diagram of a multicellular cyanobacterial filament showing the cross walls and the two rows of nozzles (small black dots) on both sides of these walls. The left cross wall has been highlighted in yellow to show the relative location of the isolated cross walls shown in **(B)** in the context of the filament. The black arrows indicate the synchronous secretion of slime from the nozzles of the same side of the cross walls, a process facilitating directed motility (Fig. S1). Figure adapted from 68. **B** A PilQ antibody labels the periphery of isolated disc-shaped cross walls (imaged by phase contrast, Ph) due to remnants of nozzle-containing longitudinal cell wall still being attached after cell breakage (Fig. S8). The data presented originate from a single experiment showing multiple labeled cross walls. **C** Following limited autolysis, clear circumferential labeling is observed at the cross walls of the *O. lutea* filament, which is absent from pre-immune sera control filaments (Fig. S9). The image series are Z-stacks representing bottom, center, and top of the filament. Filled and hollow arrow heads denote mature and nascent cross-walls, respectively. Shown are representative images of a single cell filament from an experiment that produced 19 images, capturing approximately one hundred

labeled filaments. **D** Fluorescent concanavalin A labeling (green) of live, motile *O. lutea* filaments typically showed strong adhesion of slime strands to filament surfaces. **E** Under strong lateral flow, strands of EPS slime could be detached, but the location of their source is difficult to discern due to high gliding speed of cells and rate of slime secretion. The images of **D** and **E** are from two separate experiments, capturing a total of 12 images. These images depict multiple filaments with EPS strands either wrapped around them or in various stages of detachment from the filament surfaces. **F** By subjecting *Ph. autumnale* filaments to brief sonication and cooling, individual strands of concanavalin A-labeled EPS were observed emanating from the cross walls where PilQ nozzles are located. Auto-fluorescence at the center of the cell filament is shown in red to more clearly delineate cell boundaries in this species, while the lectin-labeled carbohydrate EPS slime strands are shown in cyan. The schematic drawing on the left traces the outline of the cell filament in magenta and depicts the pattern of the lectin-labeled EPS strands as black lines. The image provides a particularly clear example of slime emanating from the cross walls, as selected from the images captured for **D** and **E**. This observation is consistent with previously documented patterns of slime secretion in filamentous cyanobacteria³³. Scale bars: **B** 2.5 μ m; **C–F** 5 μ m.

xanthus. This strategy was based on earlier observations of virtually identical nozzle-like structures in the outer membrane of this bacterium that were in close proximity to the emergence of slime bands on the surface of the cells (ref. 54; Fig. S1). To identify the nozzles from *M. xanthus*, we used a similar approach as for the cyanobacteria. Isolated cell envelopes were purified and solubilized. We examined fractions by electron microscopy to screen for the presence of structures of similar shape and size as the OM-embedded nozzles previously observed (Fig. 3A). In contrast to the nozzles from *A. platensis*, we only observed ring-shaped top views of the complex, but not side-views (compare Figs. 1E, F and 3C). Using our fractionation protocol, we isolated fractions highly enriched in nozzle-like structures, and correlated the presence of these nozzles to a ~270 kDa band on SDS-PAGE gels (Fig. 3B, C). Using mass spectrometry, the band was identified as GspD (Table S2), suggesting that secretins are also used by myxobacteria in slime secretion. Since the secretin PilQ in *M. xanthus* is known to contribute to social (S-) motility as the outer membrane channel of the

type IV pilus^{71–73}, but not gliding motility, we tested whether PilQ was also used for slime secretion in this species. Using mutants that lack PilQ, we successfully isolated nozzles and observed slime trails that were indistinguishable from the wildtype, demonstrating that PilQ is not involved in slime secretion (Fig. S10). Of note, as observed for PilQ of *A. platensis* (Fig. 1G and Fig. S4), the molecular weight of the GspD band was substantially larger than the predicted molecular weight of the mature outer membrane-associated protein (250 kDa *vs.* 90 kDa). Moreover, the secretin bands from both species displayed concentration- and temperature-dependency, with the latter being more pronounced for *M. xanthus* GspD, which completely disappeared from the gel after heating above 70 °C. Similar to PilQ, we interpret these observations to indicate that at high concentrations and/or high temperatures, these secretins irreversibly aggregate and fail to enter the gel (ref. 74, S3). In contrast, when using smaller amounts of GspD that are present in whole cell lysates and visualized by immunoblot, neither the high-molecular-weight proteins nor the temperature-

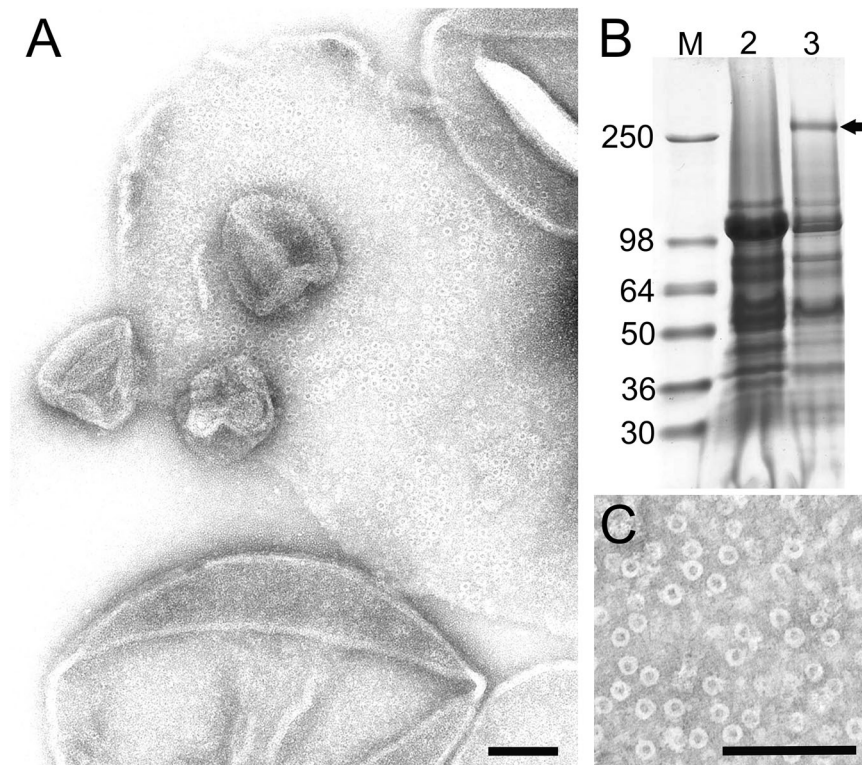


Fig. 3 | Isolation and identification of GspD in *Myxococcus xanthus*. **A** Electron micrograph of nozzle-like structures in situ in outer membrane fragments from *M. xanthus* at high magnification. The image shows a representative view of the cell pole region, compiled from dozens of independent experiments. **B** SDS-PAGE of the purified nozzle preparation showing the ~270 kDa band that is formed after heating highly concentrated samples of GspD at 70 °C. Lane 2, biochemical fraction lacking nozzles (as evaluated by electron microscopy). Lane 3, biochemical fraction containing nozzles. Arrow indicates protein band unique to fractions enriched for

nozzle-like structures, and identified as GspD (Table S2). No other protein was consistently found to co-purify with nozzle-like structures in these isolations. Size markers (first lane, M) indicate molecular weight in kDa. A representative SDS-PAGE gel from three independent experiments is shown. **C** Electron micrograph of a purified isolation of the 14–16 nm wide ring-shaped nozzle complexes formed by GspD. Scale bars: (**A**, **C**) 100 nm. This image shows a representative electron micrograph selected from multiple independent experiments. Source data are provided as a Source Data file.

dependency were observed (compare Figs. 3B and 4A). Under these circumstances, we observed a protein band at the expected molecular weight of ~90 kDa.

gspD* is an essential gene in *M. xanthus

To study a possible contribution of GspD to *M. xanthus* slime secretion, we attempted to generate a markerless deletion mutant of *gspD*. We were able to recover multiple transformants with an integrated deletion plasmid from several genetic backgrounds. However, upon counter-selection, we consistently failed to recover a deletion mutant; instead, all attempts yielded clones that had reverted to the parental wildtype strain, a result we obtained across multiple attempts in different genetic backgrounds, screening more than 3 dozen clones. We next pursued a strategy of generating a conditional knockdown mutant. For this, we introduced a second copy of *gspD* under the control of the copper-inducible promoter, P_{cuOA} at the *attB* site²⁵ into our clones that had successfully integrated the deletion plasmid. When selecting for removal of the plasmid in the presence of copper, we were able to recover multiple clones with *gspD* deleted from the chromosomal locus, with a success rate of ~25% (whereas ~75% were wildtype). These observations support the interpretation that *gspD* is an essential gene.

To test the depletion of GspD, we grew cultures in media with copper, then washed and re-suspended the cells in media lacking copper, but containing the copper chelator bathocuproinedisulfonic acid (BCS). Equal cell numbers were collected at various time points, lysed with sample buffer, and examined by immunoblot using an affinity-purified antibody against the C-terminus of GspD (see Methods for details). GspD levels declined for more than 24 h following removal

of copper before leveling off at a low, but consistently detectable, amount (Fig. 4A). This low level was not due to a small number of escape mutants, but was visualized by immunofluorescence as a weak signal in all cells present in the culture (Fig. 4B). This result was repeated independently across 4 experiments, and the expression of GspD in all cells visualized is also consistent with the expected expression pattern of an essential gene. Cells grown in the presence of copper displayed enhanced fluorescence at the periphery of the cell, in a pattern consistent with signal from endogenous GspD in wild-type cells but at levels higher than for endogenous protein (Fig. 4B). Overexpression of GspD under these conditions was similarly confirmed by immunoblot (Fig. S11). Of note, in some immunoblots, a weak cross-reacting band with a molecular weight lower than that of GspD was visible, running at either 47 kDa (Fig. 4A) or even lower molecular weights. Mass spectrometry of the corresponding SDS gel area detected GspD (Table S2), indicating that these cross-reacting bands represent a protein that underwent proteolytic degradation during sample handling - a phenomenon often observed in *M. xanthus* protein samples due to the large number of proteases of this predatory bacterium⁷⁶. This degradation cannot always be prevented, even when using a cocktail of protease inhibitors.

Consistent with the expression patterns of GspD in copper-depleted cells, we found that our *gspD* cells would grow for several generations in liquid culture in the absence of copper, but at longer times (>24 h) the growth rates of the cultures would dramatically decline. To test the requirement for copper in the media, cells were grown in the absence of copper for 48 h (the earliest observed time of maximum GspD depletion (Fig. 4A)), and serial dilutions were spotted

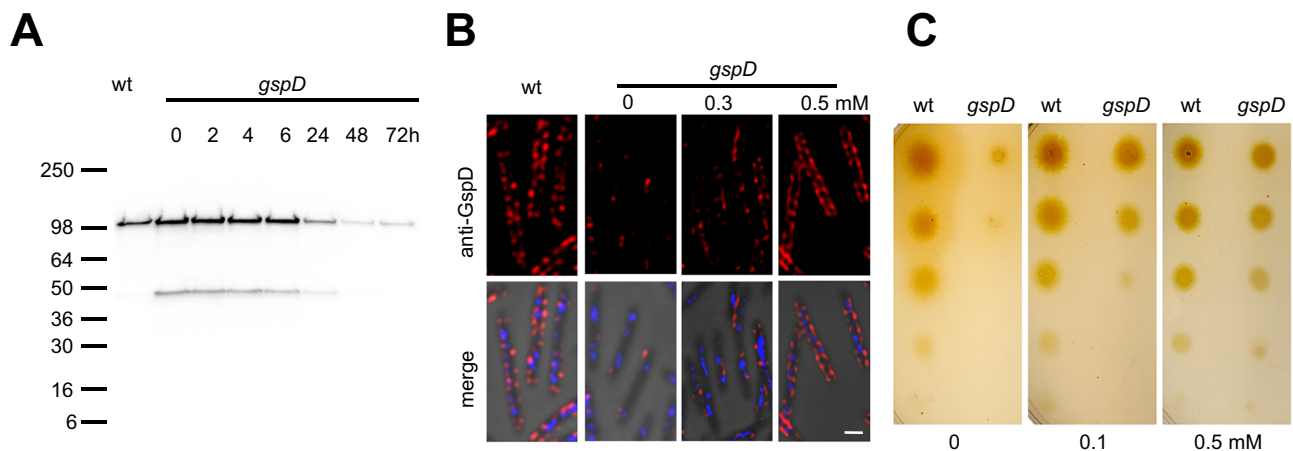


Fig. 4 | *gspD* is an essential gene in *Myxococcus xanthus*. **A** Immunoblotting reveals that removal of copper from the medium of a cell line expressing *gspD* under a copper-inducible promoter leads to a gradual decrease of GspD, which eventually stabilizes at a low but detectable level. GspD is visualized as a ~100 kDa band, with occasionally a second band at ~47 kDa or lower molecular weight. These lower-weight bands represent proteolytically degraded GspD (Table S2). Size markers (first lane) indicate molecular weight in kDa. Specific time-points post-copper withdrawal were performed once, and reliance on copper for GspD was assessed by immunoblot twice independently for each of the two mutants.

B Immunofluorescence microscopy reveals low-level expression of GspD signal in cells grown without inducer. Cells were grown in the indicated concentration of CuSO₄ for 24 h prior to fixation and imaging. Top panel, anti-GspD signal; bottom,

merged image with anti-GspD (red), DAPI (blue), and phase contrast. Images are representative of the field of cells from each growth condition, and the effects of copper depletion on GspD expression and localization were assessed by IFM in three independent experiments. Scale bar, 1 μ m. **C** Plating of wild type (wt) cells and cells containing a copper-inducible version of GspD reveal that *gspD* is an essential gene. Cells pre-cultured in 0.2 mM CuSO₄ were shifted to culture lacking CuSO₄ for 48 h. Cells were then concentrated, and 4-fold serial dilutions were spotted on agar media containing the indicated concentration of CuSO₄. In the absence of copper (left panel) the mutant strain fails to grow, while with increasing amounts of copper (intermediate concentration, middle panel; high concentrations, right panel) the cells grow at rates indistinguishable from the wild type. Source data are provided as a Source Data file.

on agar plates lacking or containing copper. We observed no effect of this handling on the survival or growth of wildtype cells, but *gspD* mutants were highly dependent on copper in the media, confirming that the cells need to express GspD in order to survive and grow (Fig. 4C).

GspD depletion yields fewer nozzles and reduced slime secretion in *M. xanthus*

To test the hypothesis that GspD is the major component of the slime nozzle, we grew *gspD* mutant cells in the absence or presence of copper. Cells were collected, and OMs were disrupted with glass beads and examined by TEM for the presence of nozzles⁵⁴. While we found a few of the complexes in the OM from cells depleted for GspD, we observed large numbers of such structures in the OM fragments from cells grown in the presence of copper (Fig. 5A).

We next wished to assay for production of slime, the A-motility-related exopolymer (AEP). Multiple methods have been reported for the detection of AEP in *M. xanthus*, including phase contrast microscopy⁷⁷, India ink⁷⁸, acridine orange⁵⁴, atomic force microscopy⁷⁹, wet-SEEC or fluorescently labeled concanavalin A⁵⁶. However, material other than AEP is produced by cells during locomotion and biofilm formation^{80–82}, which may confound results. Thus, to visualize AEP directly, we performed negative staining and examination by electron microscopy, as described⁵⁴. To observe AEP trails, we grew cells in liquid culture with or without copper for 40 h, spotted them on EM grids coated with hydrolyzed chitosan, and allowed them to glide. Grids were then stained and examined by TEM for the presence of AEP trails. We identified AEP trails as having distinct morphology (distinguishable from membrane vesicles and tubule-like outer membrane protrusions, as well as the S-motility-related EPS fibrils) in the TEM, and by their pH sensitivity, as treatment with acidic stains (un-buffered uranyl acetate (UA), pH 4.5 or SiPTA at pH 4.0) removed slime trails (but not other membrane components, i.e., vesicles) from grids, while neutral stains (SiPTA at pH 7.0) did not (Fig. S12). We consistently found that cells expressing *gspD* regularly secreted AEP, visualized as persistent and thick trails emerging from the cell body, whereas cells

depleted for GspD produced very low levels of AEP, or none at all (Fig. 5B). In these depleted cells, the only extracellular material that resembled AEP was often fragmented bands of material, thinner and shorter than AEP trails observed in wildtype or *gspD*-overexpressing cells (Fig. 5B).

We considered that the loss of the essential functions of GspD may lead to cell death, and the lack of AEP secretion we observed was simply due to observations of dead or dying cells. To address this concern, we grew cells in the presence of low, moderate, or high concentrations of copper for 24 h. We selected 24 h as the time for pre-culture, since at this time point, there is depletion of GspD from the cells, but not maximal depletion (Fig. 4A), and cells in liquid cultures did not yet show a growth defect. We selected copper concentrations that had previously demonstrated minimal toxicity to *M. xanthus* cells⁷⁵. Cells grown under these conditions were spotted on EM grids, and the numbers of AEP trails emerging from individual cells with intact membranes (to avoid sick or dead cells) were counted. Compared to the cells grown with moderate copper levels, cells grown with low levels of copper produced nearly half as many AEP trails (15 ± 7 vs. 8 ± 8 trails/cell). Moreover, overexpression of GspD resulted in a doubling of the AEP trails for cells grown in high levels of copper (32 ± 17 trails/cell; Fig. 5C). This observed GspD-dependent increase is a strong indication of the direct contribution of GspD to AEP secretion.

Three exopolymers have been characterized in *M. xanthus*: EPS, CPS, and BPS³⁴. The exopolysaccharide EPS forms fibrils that are necessary for S-motility⁸⁰, while the spore coat polysaccharide CPS is the main component of the carbohydrate coat of fruiting body spores⁸³. Finally, the recently discovered biosurfactant polysaccharide BPS mediates biofilm formation and swarm expansion on agar⁸⁴. To test whether any of these exopolymers constitutes AEP, deletion mutants for each exopolymer, as well as a triple mutant defective for all three polymers, were tested for their ability to secrete AEP. All investigated mutant strains still secreted A-motility slime, indicating that this material is distinct from all characterized *M. xanthus* exopolymers (Fig. S13).

Taken together, these data demonstrate that under conditions where GspD was partially depleted from the cells, cell survival

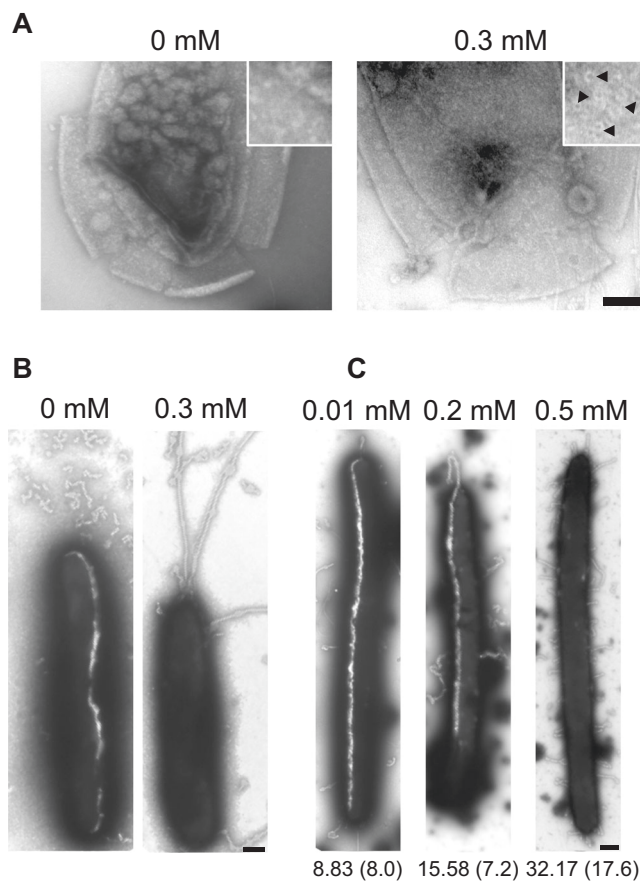


Fig. 5 | Depletion of *gspD* results in a reduction of the number of nozzles.

A Electron micrograph of negatively stained outer membrane fragments from disrupted cells, revealing few or numerous ring-shaped GspD complexes depending on the absence or presence of copper. The insets show representative areas of the outer membranes at higher magnification. Black arrows indicate GspD complexes. Scale bar, 100 nm. Cells from two independent mutants were prepared and imaged a total of three times. **B** Electron micrograph of representative cells in the absence or presence of copper. Cells that have very few GspD nozzles secrete little or no AEP slime, while cells possessing normal numbers of GspD nozzles secrete easily detectable bands of slime. **C** Cells grown in 0.2 mM CuSO_4 were shifted to the indicated concentration of CuSO_4 for 24 h. Cells were allowed to swarm on grids, and visualized by electron microscopy. For each condition, at least 12 cells were scored for the number of AEP slime trails emanating from the bodies of isolated cells with intact membranes. The mean number of slime trails per cell with S. D. in parenthesis is presented. All concentrations are mM CuSO_4 . The influence of copper on slime secretion was tested a total of 5 independent times. Scale bar, 500 nm. Source data are provided as a Source Data file.

remained unaffected, whereas AEP secretion was visibly reduced. These data support the conclusion that AEP secretion is specifically associated with the reduction of GspD. Additionally, the analysis of exopolymer mutant strains reveals that AEP is a distinct, so far uncharacterized polymer.

GspD is necessary for gliding motility in *M. xanthus*

As all models for gliding motility in *M. xanthus* suggest an important role for AEP^{58,85}, we predicted that AEP-deficient mutants should be defective in gliding. To test this, we grew cells for 24 h in media lacking copper, spotted these cells onto agar plates containing, or lacking copper, and allowed cells to swarm for 48 h. When these cells were plated onto media lacking copper, we observed cell growth from the initial, dilute spot. However, while the absence or presence of copper had no effect on the ability of wildtype cells to expand, the *gspD* mutant completely depended on copper for individual-cell motility

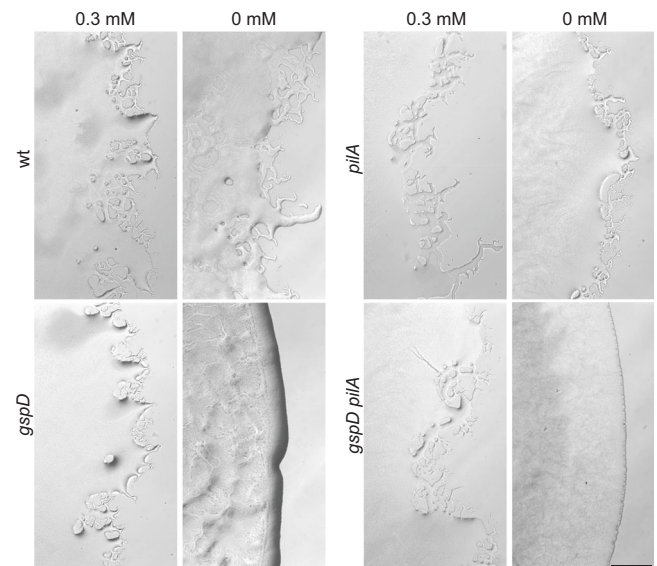


Fig. 6 | GspD is required for adventurous (A-) motility in *Myxococcus xanthus*. Appearance of the swarm colonies and edges of wild type (wt), *gspD*, $\Delta pilA$, and *gspD* $\Delta pilA$ cells in the presence and absence of copper. Single cell-based A-motility, characterized by individual cells spreading from the colony edge outwards, is observed in the wild-type cells and the $\Delta pilA$ cells. In contrast, depletion of GspD abolishes this movement in *gspD* and *gspD* $\Delta pilA$ cells, confirming that GspD is required for A-motility. The influence of copper on A motility was tested in 5 independent experiments for each mutant. Scale bar is 1000 μm .

(Fig. 6). To ensure that *gspD* expression was stimulating gliding (adventurous, or A-motility in *M. xanthus*), and not the type-4 pilus-dependent S-motility, we generated *gspD* mutants in the S-motility deficient $\Delta pilA$ background. Whereas the parent strain was able to expand in the absence or presence of copper, the *gspD* mutant required copper for motility (Fig. 6).

Since we had concluded that *gspD* is an essential gene, we tested that in this assay, the cells were living, but simply unable to glide. All of the swarm colonies became denser over the 48 h of the assay, including those that did not demonstrate motility, indicating growth of the colonies. Moreover, *gspD* cells grown under conditions similar to the gliding motility assay, but plated on soft agar to promote S-motility, demonstrated swarm expansion typical of S-motility in both the absence and presence of copper (Fig. S14A), demonstrating both that GspD was not necessary for S-motility and that even under conditions of GspD depletion, cells were still actively motile. The swarm colony was smaller for cells grown in the absence of copper, likely due to a slower growth rate of the cells from depleted levels of GspD; however, motility was clearly observed. We also collected cells from $\Delta pilA$ *gspD* swarm colonies plated in the absence or presence of copper, and determined cell viability. We observed no differences in the ratio of living to dead cells (Fig. S14B), suggesting that the cells that survived the copper depletion expressed enough GspD to survive, but not to swarm (Fig. 4A). Taken together, these results demonstrate that cells sufficiently survived the depletion of GspD in these experiments, and that swarm expansion could have been detected had it occurred. Thus, we conclude that *gspD* is an A-motility gene, which may not have been identified in previous genome-wide genetic screens (reviewed in ref. 86) because it is an essential gene.

Discussion

EPS secretion is an important strategy for environmental adaptation of bacteria⁸⁷. With enormous diversity in chemical and physiological properties, these molecules serve a wide variety of purposes, including as important components of the bacterial cell envelope^{7,30,34}, providing

protection against desiccation and toxic substances^{87–89}, mediating attachment to surfaces^{87,90}, biofilm formation^{91,92}, host interaction^{93,94}, and bacterial motility^{58,60}. Although there are many methods for the detection of bacterial EPS, relatively little is known about the chemical composition, synthesis, and secretion of these molecules.

Here we identify the previously observed EPS-secreting nozzles in cyanobacteria⁵³ and myxobacteria⁵⁴ as the secretins PilQ and GspD, respectively (Fig. S1). As Gram-negative bacteria can possess multiple envelope-associated macromolecular secretory complexes, it was essential to ensure that the ring-shaped molecules we isolated were indeed the slime nozzles. For this reason, we initially used the cyanobacterium *A. platensis*, which, as a photosynthetic autotroph, is capable of EPS production while having relatively few secretory systems that may have been mistaken for nozzles. In fact, BLAST searches reveal that none of the three cyanobacteria species we used contain transport systems with large outer membrane gate structures such as T3SS, T4SS, and T6SS. Only Wza homologs are found, which are substantially smaller than the nozzles (outer diameter 4.6 nm in *E. coli*⁴⁰). In line with these observations, isolations from *A. platensis*, *O. lutea*, and *Ph. autumnale* invariably yielded a single type of ring-shaped complex formed by PilQ, allowing identification of secretins as the principle structural component of the slime nozzles of filamentous cyanobacteria. This interpretation is supported by immunoblot analyses (Fig. S4), mass spectrometry (Table S2), structural comparisons with known secretin complexes (Fig. S7¹⁰), integrative cryo-EM and AlphaFold 3D reconstruction (Fig. 1H), immunofluorescence microscopy of *O. lutea* and *Ph. autumnale* filaments (Figs. 2 B, C; S8), and the correlation of the localization of PilQ (by immunolabelling) with the nozzles (by electron microscopy) to isolated cross walls or whole cell filaments (compare Fig. 2B and Fig. S8 for a single isolated cross wall or Figs. 1B and 2C for a whole filament).

Unlike the three studied cyanobacteria, the predatory myxobacteria^{95,96} possess copies of virtually all known Gram-negative protein secretion machineries⁹⁷. In fact, the genome of *M. xanthus* contains 3 paralogs of *gspD*, namely *gspD*, *pilQ*, and *mxan_RS15055* (previously *mxan_3106*)⁹⁷, with the greatest sequence similarity within the secretin domain (Fig. S15). All three paralogs have been identified in proteomics studies as expressed and localized to the OM or OM vesicles of *M. xanthus* cells under various environmental conditions⁹⁸. PilQ is the outer membrane secretin of the type IV pilus⁷², while Mxan_RS15055 (Om031 in *M. fulvus*) has been reported to be involved in osmoregulation, allowing cells to better survive under increasing salinity⁹⁹. Our isolations of slime nozzles fortuitously contained only one type of ring-shaped complex, namely the secretin GspD (Fig. 3B, C and Table S2), which were also isolated from mutants lacking *pilQ* (Fig. S10). Depleting GspD from *M. xanthus* resulted in a reduction in AEP secretion (Fig. 5). Together, these data support the conclusion of GspD as the slime nozzle in *M. xanthus*, and show that the three paralogous secretins have distinct functions and that the role of GspD in AEP secretion and A-motility is unique.

The identification of these nozzles as secretins was consistent with their electron microscopic appearance¹⁰. However, the presence of the second protein in cyanobacteria, the pentapeptide repeat protein NIES39_A07680, was unexpected. Pentapeptide repeat proteins, categorized under Pfam 00805, are particularly prevalent in cyanobacteria and have been implicated in unknown targeting or structural functions¹⁰⁰. NIES39_A07680 co-purified with PilQ, and its high-confidence AlphaFold-predicted structure aligns well with the large lower ring part of the isolated nozzle complexes, a feature absent in other secretins (Figs. 1H; S7). Its compact size and the presence of multiple repetitive putative protein-protein interaction motifs, specifically pentapeptide repeats¹⁰⁰ instead of TPR¹⁰¹ indicate that NIES39_A07680 bears no resemblance to known pilotins or secretin accessory proteins²⁰. Therefore, it may represent a cyanobacteria-specific secretin-associated protein. Another unexpected finding was

that the nozzles recovered from cyanobacteria were almost entirely dimers of PilQ rings (in one count, 615 out of 618 structures were dimers), mirroring earlier observations (333 out of 334 structures⁵³). Despite their initial visual differences (compare Figs. 1E and 3C), the adsorption of *A. platensis* nozzles to grids without glow discharge revealed top views that clearly exposed the common ring-shaped architecture of the nozzles (compare Figs. 1F and 3C). Two possible scenarios were considered to explain the distinct appearance of cyanobacterial nozzles: either the physiological structures are monomeric rings, and the observed dimers formed during isolation, or the nozzles function as dimers, indicating a plasticity in certain secretins to adopt novel structural arrangements. In contrast to cyanobacterial nozzles, those from myxobacteria were exclusively recovered as single-ring structures, with no additional proteins co-purified. This observation supports the first interpretation, suggesting that the nozzles in cyanobacteria exist as monomeric rings lacking conventional associated proteins or pilotins when fully assembled. The visualization of PilQ dimers was likely an artifact of the sample preparation. The role of NIES39_A07680 may involve facilitating the arrangement of the nozzles in rows by acting as a molecular spacer between individual complexes or physically reinforcing the nozzle to withstand the possible pressure due to the expansion of the carbohydrate cargo. Given that this spatial arrangement and physicochemical properties of the cargo are unique to cyanobacteria, there may not be a requirement for a comparable protein in other bacterial secretin complexes. To resolve this question, a detailed examination of isolated or in situ *A. platensis* nozzles and a functional analysis of NIES39_A07680 may be necessary.

To explain the dependence of slime secretion on the presence of secretins, we consider two plausible mechanisms: secretins could either be directly involved in slime secretion as the OM gates through which the synthesized polymer is secreted, or indirectly by secreting enzymes that then polymerize slime on the cell surface, similar to the synthesis of bacterial dextrans³⁰. In dextran production, secreted surface-associated transglycosylases enzymatically cleave extracellular sugar polymers such as sucrose, starch, or fructans to convert the resulting monosaccharides into dextran polymers. To consider whether such a process could account for slime polymerization in our organisms, we evaluated the repertoire of secreted proteins. In *M. xanthus*, GspD has recently been shown to translocate MYXO-CTERM domain-containing proteins¹⁰², of which 34 have been bioinformatically identified using the TIGR03901 consensus motif¹⁰³. Only one of those 34 proteins, MtsC (Mxan_RS06455, MXAN_1334¹⁰⁴) is involved in motility, but not A-motility. None of the five MYXO-CTERM domain-containing proteins, (Mxan_RS04600, MXAN_6274, PQQ-dependent sugar dehydrogenase; Mxan_RS30220, MXAN_6236, putative polysaccharide degrading enzyme; Mxan_RS30405, MXAN_6274, polysaccharide deacetylase family protein; Mxan_RS34095, MXAN_7044, exo- α -sialidase; Mxan_RS34570, MXAN_7140, glycosyl hydrolase) that are involved in carbohydrate metabolism show similarity to transglycosylases. Moreover, the CTT media used does not contain cleavable sugar polymers, and physiological experiments have shown that *M. xanthus* is unable to utilize glucose, starch, or glycogen from the medium¹⁰⁵. We therefore reason that it is unlikely that the AEP slime in *M. xanthus* could be synthesized using an extracellular transglycosylase reaction³⁰. Supporting this conclusion, no transglycosylases (or indeed, any proteins) have been identified as PilQ substrates that could polymerize slime outside of the filamentous cyanobacteria. BG11 medium, like CTT, does not contain any carbohydrates that could act as substrates for transglycosylase-like enzymes. To allow extracellular polymerization in the absence of cleavable carbohydrate precursors would necessitate the secretion of large quantities of activated UDP-sugars by the bacteria. However, no such polymerization process has been reported in any bacterium, and the unavoidable loss of UDP would make such a process metabolically extremely costly. Therefore, we consider the most plausible interpretation of our findings to be that

the role of the secretins is to secrete polymeric slime. While this reasoning is highly plausible for the cyanobacterial EPS, which has been previously shown to be a complex heteropolysaccharide⁵⁵ and is stainable with the carbohydrate-binding lectin concanavalin A in *O. lutea* (Fig. 2D–F), the evidence for the carbohydrate nature of AEP in *M. xanthus* is less compelling. Although it has been reported that AEP was visualized with fluorescently labeled concanavalin A⁵⁶, we have been unable to replicate this in our *M. xanthus* strain DK1622. Furthermore, the previous experiments did not rule out the fluorescent labeling of other extracellular material. Unlike in the filamentous cyanobacterium *P. uncinatum*, the slime in *M. xanthus* has not yet been purified, and its chemical composition remains unestablished.

The discovery that bacteria use secretins as the OM gate for EPS secretion prompts the question whether this mechanism represents a completely novel type of EPS secretory pathway, or whether the secretin is used as the OM component of other, already known, EPS secretion systems^{7,30}. We also do not yet know all proteins involved in the synthesis, polymerization, and trans-periplasmic transport of slime. Nonetheless, evidence from cyanobacteria indicates that slime secretion may involve a synthesis-dependent mechanism. The secreted EPS slime in *P. uncinatum* is a complex heteropolysaccharide⁵⁵, and recent genetic work has identified a highly conserved, 13 gene-long locus that is important for EPS secretion and motility in all sequenced filamentous cyanobacteria¹⁰⁶. The *hps* locus encodes five glycosyltransferases (*hpsEFG, I*, and *K*) and four pseudopilins (*hpsBCD* and *H*), among others. The involvement of these genes suggests a potential link to secretins, as pseudopili act as pistons to push protein cargos through the OM secretin gate²². Therefore, it is tempting to speculate that the *hps* locus encodes parts of a novel synthase-dependent system that secretes EPS slime using PilQ as the OM gate.

The finding that GspD in *M. xanthus* is potentially involved in two very different secretory processes, namely AEP slime and protein secretion, raises the intriguing possibility that the same OM channel might engage multiple accessory protein complexes in the periplasm and cytoplasmic membrane. It is possible that GspD is not limited to only these two activities, and is involved in additional transport processes, such as the release or uptake of low-molecular-weight substances, a possibility that is supported by observations of the diffusion of small molecular weight substrates through closed secretins^{25,107}. Because of these multiple activities, our finding that *gspD* is an essential gene does not necessarily lead to the conclusion that slime secretion is essential to survival, as the secretion of the MYO-CTERM domain-containing proteins would also be disrupted (and any other cell envelope machinery that relies on GspD). This potential versatility may also explain the apparent mismatch between the number and distribution of GspD nozzles across the cell body and the observed AEP slime bands emerging from the cell surface. When grown on hard agar, an average cell possesses about 250 nozzles per pole⁵⁴, with a somewhat lower number distributed along the cell body; where we observed fewer AEP slime bands (see e.g., Fig. 5B). A substantial number of GspD secretins may therefore participate in protein secretion alone, or alternatively, multiple nozzles may contribute to the formation of each slime band. Further study investigating if specific GspD-associated activities are organized spatially into specific sub-domains across the cell would help resolve this question.

An important aspect of EPS and AEP secretion in cyano- and myxobacteria, respectively, is their putative role in gliding motility in these organisms^{54,60}. Although an important role for slime secretion for motility is generally accepted⁵⁸, its exact contribution is a matter of debate ranging from a passive adhesion factor⁵⁶, to a viscoelastic substrate⁸⁹, to a propulsive force generator^{52,53}. What complicates resolving these issues is the possibility that the contribution of slime secretion to motility may be different in different bacteria. For the normally non-motile cyanobacterium *N. punctiforme*, hormogonia (short, transiently motile filaments) were recently reported to use

slime secretion and type IV pilus-related proteins in gliding motility¹⁰⁸. Based on the finding that mutant strains lacking multiple glycosyltransferases (*HpsE-G*) were deficient in motility, and the observation that media conditioned by wild-type hormogonia could restore motility in these mutants, it was suggested that slime secretion facilitates motility but does not generate the motive force for gliding in *N. punctiforme* hormogonia¹⁰⁸. Notably, we have never observed assembled type IV pili in permanently motile filamentous species such as *O. lutea* and *Ph. autumnale*, nor in previously studied cyanobacteria of the genera *Oscillatoria*, *Phormidium*, *Lyngbya*, and *Anabaena*^{53,59,109,110}. This suggests that these species lack functional pili, but still possess the conserved *hps* locus¹⁰⁶. We suggest that these species may synthesize slime similar to *N. punctiforme*, but may use their secretin PilQ directly for its secretion. Moreover, the absence of pili precludes that either retraction (like in *Synechocystis* or *Myxococcus*) or extension (as suggested for *N. punctiforme*) of these structures could power movement in the vast majority of filamentous cyanobacteria. An important unresolved question in this context is whether parts of the type IV pilus machinery, such as the minor pilins and the pilin PilA, act as a piston to push the EPS slime out of the PilQ gate, as has been suggested¹⁰⁸. The identification of PilQ/GspD as a slime nozzle is, therefore a necessary first step to allow testing these various hypotheses on the contributions of slime secretion to motility in these various bacteria. In this context, our observations of GspD-depleted cells clearly demonstrate that AEP slime secretion contributes to gliding motility in *M. xanthus*. Thus, we provide direct molecular evidence that slime contributes to motility and identify *gspD* as a bona fide A-motility gene. Moreover, that *gspD* is essential also explains why the nozzle has so far never been identified in genome-wide genetic screens⁹⁰, and suggests the possibility that additional key components of A-motility remain to be found.

Alone, our results do not address the debate about the role of slime secretion in A-motility, since all current models propose a requirement for slime secretion. If slime secretion provides the propulsive force for motility, cells lacking slime secretion should lack A-motility, but the same would be true if slime is an important adhesion that provides surface contacts necessary for other molecular motors to act on⁸⁹. Therefore, additional experiments are required to address the precise role of slime secretion in A-motility; for example, the analysis of the chemical composition of the slime and its physico-chemical properties, the identification and deletion (or depletion) of genes involved in its synthesis, and the determination of whether cells must themselves secrete slime to be motile, or simply require slime in their environment (as is true of *N. punctiforme* hormogonia¹⁰⁸). Equally important will be to answer how widespread is the use of secretins as high-throughput nozzles for EPS secretion in Gram-negative bacteria.

In this study, we provide evidence for the identity of the OM slime secretion nozzles in cyanobacteria and myxobacteria as the T2SS secretins PilQ and GspD, respectively. These findings demonstrate a novel and conserved activity for secretins across genetically diverse species, and suggest that secretins may serve multiple roles as an OM gate in Gram-negative bacteria. We further demonstrate that slime secretion is necessary for A-motility in *M. xanthus*. With the identification of an essential part of the slime secretion apparatus, we now provide a target for generating genetic tools that can address the long-predicted roles of slime secretion in gliding motility for these organisms.

Methods

Bacterial strains and growth conditions

M. xanthus cells were grown in CTT (1% casitone, 10 mM Tris pH 8.0, 8 mM MgSO₄, 1 mM KH₂PO₄) or 1/2 × CTT (0.5% casitone, 10 mM Tris pH 8.0, 8 mM MgSO₄, 1 mM KH₂PO₄) and maintained on CTT plates with 1.5% agar⁷¹. When appropriate, 100 µg/ml kanamycin or 15 µg/ml oxytetracycline was used for selection. *A. platensis* strain LB 2340 from the Texas Algal Culture collection UTEX was grown under constant white light using an alkaline *Spirulina* medium: solution I (162 mM

NaHCO₃, 38 mM Na₂CO₃, and 2.9 mM K₂HPO₄ in 500 ml dH₂O) and II (29.4 mM NaNO₃, 5.74 mM K₂SO₄, 17.1 mM NaCl, 0.81 mM MgSO₄, 0.27 mM CaCl₂ in 500 ml dH₂O) were autoclaved separately, combined after cooling, and 2 ml of a sterile-filtered 0.1 mM vitamin B₁₂ solution was added. The freshwater cyanobacteria *O. lutea* (UTEX 1814) and *Ph. autumnale* (strain ATFG6; isolated by Dr Aya Farag from the University of Sheffield from a drainage site in Chesterfield, UK, and identified by 16S rRNA sequencing¹¹¹) were grown in BG11 medium (17.6 mM NaNO₃, 0.23 mM K₂HPO₄, 0.3 mM MgSO₄, 0.24 mM CaCl₂, 0.031 mM citric acid, 0.021 mM ferric ammonium citrate, 0.0027 mM Na₂EDTA, 0.19 mM Na₂CO₃, 1 ml trace metal mix per 1000 ml dH₂O). Both strains, *O. lutea* and *Ph. autumnale* were sequenced by MicrobesNG (Birmingham). Strains used are listed in Table S3.

Construction of copper-inducible mutants

To generate a markerless deletion of the *gspD* gene, plasmid pDMZ96 was generated. A deletion cassette with sequence upstream and downstream of *gspD* was generated by overlap PCR using primers Δ2514 EcoRI A and Δ2514 B for the upstream fragment, and Δ2514C and Δ2514D for the downstream fragment (Table S4) using Pfu Ultra polymerase (Agilent, Santa Clara, CA) and the DK1622 strain of *M. xanthus* as template. Amplicons were gel-purified, and amplified by PCR with primers Δ2514A and Δ2514 BamHI D. The deletion cassette was digested with EcoRI and BamHI (New England Biolabs, Ipswich, MA) and ligated to similarly digested pBJ114. The sequence was confirmed by Sanger sequencing. pDMZ96 was transformed to each parent cell line (Table S3) and selected for plasmid integration with 100 μg/ml of kanamycin. Clones were selected and grown in media lacking kanamycin, plated in media containing 2.5% galactose to select for loss of the plasmid, and screened by PCR for gene deletion. Multiple attempts to delete *gspD* in several genetic backgrounds failed; consistent with the conclusion that *gspD* is an essential gene. As a secondary strategy, clones that had integrated the deletion plasmid were transformed with plasmid pDMZ94, which expresses the *gspD* gene regulated by the copper-inducible promoter *P_{cuoA}* from the Mx8 phage attachment site. pDMZ94 was generated by amplification of the *gspD* coding sequence from DK1622 genomic DNA using primers 2514 5' XbaI and 2514 3' stop BamHI (Table S4). Gel-purified amplicons were ligated to linearized pMAT3⁷⁵. Clones were collected and grown in media containing 300 μM CuSO₄ and subject to galactose selection. Multiple clones containing the *gspD* deletion at the native chromosomal locus were recovered and maintained in CTT media supplemented with 300 μM CuSO₄.

Construction of deletion mutants

The in-frame Δ*exoA-I* and Δ*epsD* gene deletions in *M. xanthus* were generated using homologous recombination and galactose-mediated counter selection methods as described in detail elsewhere^{112,113}. Briefly, an approximately 1000 bp-long insert containing 500 bp upstream of the first six codons of the deleted genes was fused in frame to the last six codons, and a 500 bp-long region downstream of the last gene. This insert was then cloned into the multiple cloning site of the pBJ114 plasmid. *M. xanthus* cells were electroporated with the plasmid, and plasmid integration was selected on CYE agar plates containing 100 μg ml⁻¹ kanamycin. Individual clones were plated for single colonies on CYE plates containing 2.5% galactose. Resulting colonies were confirmed to be kanamycin-sensitive. Clones bearing the desired deletion were screened by PCR¹¹⁴. At least three independent clones of the mutants were tested to confirm the phenotype.

Isolation and Purification of PilQ/GspD Nozzles

To isolate nozzles from the three cyanobacteria species, ca. 100 g wet weight of cells were harvested by centrifugation (10 min at 1000 × *g*), washed twice in Tris-HCl buffer (10 mM Tris-HCl, pH 7.5), and chilled

on ice. Cells were disrupted by glass beads using a Desintegrator S cell mill (Bernd Euler Prozesstechnik, Frankfurt) at 0 °C, and unbroken cells were removed by low-speed centrifugation (10 min at 1000 × *g*). Crude cell envelopes were collected on ice and further purified using a Percoll density gradient (15% vol/vol) for 1 h at 10,000 × *g*. The pale orange-colored pellet at the bottom of the gradient contained highly enriched cell envelopes. After several washes with Tris buffer, the purified envelopes were re-suspended in the buffer containing 2% Triton X-100 and 0.02% sodium azide. The suspension was shaken overnight at 37 °C and the autolytic digestion of the peptidoglycan monitored by light microscopy. Undigested cross walls and debris were removed by centrifugation (10 min at 50,000 × *g*) and crude nozzle preparations were collected in the ultracentrifuge (1 h at 366,000 × *g*) before being further purified using a CsCl density gradient (0.3 g/ml). After overnight centrifugation, the band containing the nozzles was collected using a gradient fractionator (Labconco Auto Densi-Flow), dialyzed against Tris buffer, and the nozzles were either collected by centrifugation (1 h at 366,000 × *g*) or further purified using 30 ml gradients of 10–40% sucrose (wt/wt). One milliliter of the nozzle-containing suspension was dialyzed against Tris buffer and then layered on top of the gradient and centrifuged at 100,000 × *g* for 17 h using a Beckman SW41 rotor. The twelve collected fractions were dialyzed against Tris buffer, examined in the electron microscope for the presence of nozzles using carbon-coated copper grids that were either glow-discharged or not, and analyzed using SDS-PAGE. Proteins were identified using Edman degradation and mass spectrometry.

To isolate GspD nozzles from *M. xanthus*, ca. 80 g wt or Δ*pilQ* cells were collected by centrifugation and re-suspended in 1 M sucrose by vigorous shaking. Cells and cell debris were removed by differential centrifugation (17,000 × *g* for 10 min followed by 32,000 × *g* for 10 min), and five volumes of chilled Tris buffer were added to dilute the sucrose. Enriched OMs were pelleted by centrifugation (10 min 50,000 × *g*) and re-suspended in Tris buffer at a concentration of 0.1 g/ml. An equal volume of 1% solution of dodecyl-maltoside was added to solubilize the OMs, and un-solubilized material was removed by centrifugation (10 min 50,000 × *g*). After addition of 0.3 mg/ml CsCl, the solution was centrifuged overnight at 366,000 × *g* using a Beckman SW 55 Ti rotor. A turbid yellowish band was visible about 2/3 of the way in the gradient and was identified as enriched in nozzle-like structures by TEM. These nozzle-containing bands were harvested, dialyzed against Tris buffer, and either directly analyzed or further purified as described above for the cyanobacteria.

Antibody production and quality control

His-GspD and His-PilQ_{OUT} were expressed in *Escherichia coli* BL21 cells and purified using Nickel-NTA agarose beads (Qiagen, Germantown, MD) according to the manufacturer's instructions. The proteins were injected into rabbits to generate polyclonal antibodies according to standard protocols (His-GspD, Cocalico, Reamstown, PA; His-PilQ_{OUT}, Eurogentec, Seraing, BE). Sera were tested for cross-reactivity by immunoblotting lysates from wildtype *M. xanthus* or cyanobacterial cells, respectively. To increase the specificity of the reactivity, we affinity-purified the His-GspD antibodies. A plasmid was constructed using the pGEX 2T vector (GE Healthcare, Laurel, MD) ligated to a PCR amplicon generated using primers GspD BamHI aa 710 s and GspD aa863 stop EcoRI (Table S4) and pDMZ94 as the template. Amino acids 710–863 of GspD were expressed as a C-terminal fusion to the glutathione S-transferase protein (GST-GspD C-term) in *E. coli* BL21 strain, and captured with glutathione sepharose beads (GE Healthcare). Protein was eluted with 10 mM glutathione in 50 mM Tris, pH 8.0, 5% glycerol, and examined for purity by SDS-PAGE and Coomassie staining. Five hundred micrograms of protein were dialyzed against binding buffer (PBS with 10 mM EDTA) and re-bound to glutathione sepharose beads. Protein was then crosslinked to beads with 5 mg/ml DTSSP (Thermo Fisher Scientific, Waltham, MA) in binding buffer for 45 min at

RT. Buffer was drained and the reaction quenched by washing beads twice for 5 min with 100 mM Tris, pH 8.0. The beads were then washed extensively with binding buffer, and elution buffer (4 M MgCl₂) to remove any un-crosslinked protein. Beads were normalized with binding buffer, and incubated with the antisera overnight at 4 °C. Sera were drained, and beads washed twice with wash buffer (10 mM Tris, pH 7.5, 0.2% deoxycholic acid) and twice with wash buffer plus 0.5 M NaCl. Bound antibody was eluted with elution buffer, and collected in 1 ml fractions in tubes containing 50 µl of 10 mg/ml bovine serum albumin, and transferred immediately to dialysis bags and dialyzed against 1 L of PBS plus 0.02% sodium azide. Antibodies were tested for activity by immunoblot against lysates from *M. xanthus* or nozzle-enriched fractions from the cyanobacterial cell envelope preparations, and recognized a single band. Affinity purification was not necessary for the cyanobacterial antibody as it recognized only a single band in our species. In some secretin isolations, more than one antibody cross-reacting band was found, always with a lower molecular weight ranging from ~16–50 kDa. To test whether these bands represented non-secretin proteins cross-reacting with the antibody, identical protein samples were separated on SDS gels. These identical lanes were then either stained with Coomassie or transferred onto nitrocellulose and probed with the anti-GspD antibody. Next, the areas of the SDS gel lanes corresponding to the cross-reacting bands on the nitrocellulose were cut out and analyzed using mass spectrometry. In each case, the secretin protein was detected, supporting the interpretation that the cross-reacting bands represent proteolytically digested secretin.

SDS-PAGE, Immunoblotting, and mass spectrometry

Equal cell numbers from liquid-grown cultures or equal amounts of CsCl fractions were solubilized in 2× Tris-Glycine SDS buffer (Life Technologies) by boiling for 15 min or heating at various temperatures. Samples were separated by SDS-PAGE and transferred to a PVDF membrane (Millipore, Billerica, MA). The membrane was blocked with PBS containing 0.5% tween (PBST) and 5% milk, and probed overnight with affinity-purified anti-GspD or anti-PilQ in PBST plus 3% BSA. The membrane was washed with PBST, and probed with HRP-conjugated anti-rabbit antibody (Jackson ImmunoResearch, West Grove, PA) in PBST containing 5% milk. HRP was activated using SuperSignal West Pico Chemiluminescent Substrate (Thermo Scientific, Rockford, IL) and imaged with a FluorChem Q system (Protein Simple, Wallingford, CT). Mass spectrometry (MS)-targeted gel bands were excised, followed by three rounds of de-staining with 200 mM NH₄CO₃ in 40% acetonitrile at 37 °C for 3 min each. A final de-staining step was performed in methanol. Proteins were alkylated with 55 mM iodoacetamide for 20 min at RT in the dark and then digested overnight at 37 °C using 0.02 µg/ml trypsin. Peptides were extracted using solutions of formic acid (3.5% and 5%) in acetonitrile (30% and 50%, respectively), vacuum-dried, and stored at –20 °C. Nanoflow LC-MS/MS was conducted using an Orbitrap Elite hybrid mass spectrometer (Thermo Fisher Scientific, Waltham, MA) with a nanospray ionization source, coupled to an Ultimate RSLCnano LC System (Thermo Fisher Dionex, Sunnyvale, CA). Desalted peptides were separated on an EASY-Spray PepMap C18 column (50 cm × 50 µm ID, 2 µm particles, 100 Å pore size) using a linear gradient of 5% to 35% buffer B (0.5% formic acid in 80% acetonitrile). The Orbitrap Elite operated with a data-dependent acquisition mode. Full-scan MS spectra were acquired in the Orbitrap at a resolution of 120,000 at m/z 400. The top 20 most abundant multiply charged ions (2+ and higher) were selected for MS/MS fragmentation in the linear ion trap. An FTMS target value of 1 × 10⁶ and an ion trap MSn target value of 1 × 10⁴ were used, with the lock mass (445.120025) enabled. Maximum accumulation times were set at 200 ms for FTMS and 50 ms for MSn scans. Dynamic exclusion was enabled, with a repeat duration of 45 s, an exclusion list size of 500, and an exclusion duration of 30 s. Raw MS data were processed using MaxQuant software (version

1.6.10.43¹¹⁵) and searched against the organism's protein database (downloaded from UniProt). Search parameters included the following: Trypsin/P as the enzyme (allowing up to 2 missed cleavages), methionine oxidation and N-terminal acetylation as variable modifications, and cysteine carbamidomethylation as a fixed modification. Since the original measurement results were provided in Excel format, which is incompatible with the PRIDE database, the ProteinGroups.txt files generated by MaxQuant were used to recalculate the data and generate PRIDE-compliant files. Data are available via ProteomeXchange with identifier PXD066729. Early identifications of PilQ and NIES39_A07680 were based on MS/MS spectra and the MaxBP parameter, both of which are no longer in use and therefore could not be converted into PRIDE-compatible formats. These results are instead provided as original reports (Supplementary Data 1).

Electron microscopy of bacterial cells

To visualize slime secretion, carbon-coated gold grids (EMS) were glow-discharged, coated with acid-hydrolyzed chitosan⁵⁶, and dried. Grids were held face-up by forceps, and 2 µl of a suspension of cells grown in the absence or presence of copper were spotted onto the grid. Cells were incubated at room temperature (RT) in a humidity chamber for 20 min. Grids were rinsed with H₂O and routinely stained with 1.5% silico phosphotungstic acid (SiPTA) at pH 7.4. To differentiate non-slime material, grids were alternatively stained with either unbuffered uranyl acetate (UA) at pH 4.5 or SiPTA adjusted to pH 4.0 using citric acid. Grids were examined with a Hitachi 7600 or a Philips CM120 transmission electron microscope at 80 kV, and micrographs collected using AMT Image Capture Engine software controlling an AMT ER50 5-megapixel CCD camera (Advanced Microscopy Techniques Corp., Danvers, MA).

To quantify the number of slime trails per cell, EM grids were prepared as above using cells grown for 24 h in liquid media containing 0.01, 0.2, or 0.5 mM CuSO₄. Prepared grids were examined by EM, and isolated cells (>1 full cell-length from nearest neighboring cell) were selected at low magnification, so that slime trails could not be observed prior to imaging (to reduce experimenter bias). High magnification images were collected, and the numbers of slime trails emanating from at least 12 cells/condition were counted. Cells with disrupted OM were excluded. The average length of cells did not significantly vary between the populations (determined by one-way ANOVA (mean ± S.D.: 0.01 mM CuSO₄ = 9 ± 2 µm; 0.2 mM CuSO₄ = 11 ± 4 µm; 0.5 mM CuSO₄ = 9 ± 2 µm)). Data are presented as the mean number of slime trails per cell, with the standard deviation.

To disrupt OM for visualization of nozzles, cells swarming on hard agar with or without copper were scraped onto CTT media in a 1.5 ml centrifuge tube. An equal volume of 710–1180 µm glass beads was added (Sigma-Aldrich, St. Louis, MO), and samples were subjected to vortexing at maximum power for 2 min. Cells were applied to a glow-discharged EM copper grids, stained with 2.5% UA and imaged as above.

Cryosubstitution of cyanobacterial cells was performed as described⁵⁹. Briefly, *A. platensis* cells were high-pressure frozen using a Leica EM PACT2 instrument (Leica Microsystems, Buffalo Grove, IL), cryo-substituted for 80 h at –87 °C in acetone containing 2% osmium tetroxide, and, after slowly warming to RT, embedded in Spurr's resin. Thin sections were stained with 2% UA and lead nitrate¹¹⁶, and examined in a Philips CM12 electron microscope. To visualize nozzles in membranes, isolated outer membranes were picked up on 200 mesh carbon-coated copper grids and unilaterally shadowed with platinum-carbon (Pt/C) at an angle of 45°. Images at various magnifications were recorded as described above.

Negative stain electron microscopy and image analysis of isolated PilQ nozzles

CsCl gradient fractions containing cell envelope proteins of *A. platensis* were adsorbed for 30 to 60 seconds onto 400-mesh carbon-coated copper grids before being stained with 2% UA and viewed

under the electron microscope. For image analysis, a total of 1605 single, double, or multiple PilQ complexes were selected using PyTom, classified through iterative multivariate statistical analysis (MSA), and aligned using a single reference dimer particle¹¹⁷. For MSA, twelve eigenvectors were used to classify the particles into four separate classes, which were then aligned and averaged using the TOM toolbox programs¹¹⁸.

Cryo-EM grid preparation and data collection

PilQ nozzle-enriched CsCl gradient fractions were dialyzed overnight against Tris buffer (10 mM Tris-HCl, pH 8.0) at 4 °C and incubated with about one-fifth of the volume of DEAE Sepharose (Sigma) equilibrated with Tris buffer for 30 minutes. The Sepharose was removed through centrifugation, and 4 µl aliquots of the supernatant were pipetted onto glow-discharged C-flat holey carbon film R 1.2/1.3 400 mesh Quantifoil grids (EM Sciences, Hatfield, PA). An EM GP cryopreparation system (Leica Microsystems, Buffalo Grove, IL) was used for plunge-freezing with the following parameters: 5 s pre-blot time, 2.0–5.0 s blotting time, followed by 0.5 s post-blot time. Cryo-EM data were collected on a Tecnai Arctica (FEI, Hillsboro, OR) at 200 kV, utilizing an energy filter and a direct electron detector (Gatan, Pleasanton, CA) operated by EPU software (Thermo Fisher Scientific, Waltham, MA). Images were recorded at a defocus range of −1.0 to −2.6 µm using a total dose of 40 e[−] Å^{−2} per micrograph.

Cryo-EM data processing and model building

CryoSPARC (v4.3.1) was used for all CryoEM data processing steps¹¹⁹. After patch motion correction and patch CTF correction, 13,642 particles were picked from 313 micrographs. 2D classification resulted in 5 classes with a total of 1505 particles. Ab-initio 3D reconstruction converged to a volume with C-16 symmetry. Non-uniform refinement was performed with C-16 symmetry enforced, resulting in a reconstruction with a gold-standard FSC resolution of 4.04 Å. Visualization and reconstruction manipulation were performed using ChimeraX version 1.7¹²⁰.

Immunofluorescence (IF) Light Microscopy

M. xanthus were grown 24 h in the absence or presence of 300 µM CuSO₄ and adhered to sterile glass coverslips overnight in CTT media, with or without copper. Cells were then processed essentially as described⁷⁶. Briefly, cells were rinsed with PM buffer (20 mM Na-phosphate, 1 mM MgSO₄, pH 7.4) and fixed with 4% paraformaldehyde in PM buffer. Cells were permeabilized with 0.2% Triton X-100 and 1 mg/ml lysozyme, and probed with affinity-purified anti-GspD antibody at a 1:10 dilution in PBS buffer with 2% BSA. Secondary antibody was Alexa594-conjugated anti-rabbit (Life Technologies, Carlsbad, CA) diluted 1:1000 in PBS with 2% BSA. Cells were stained with 1 µg/ml DAPI (Sigma-Aldrich, St. Louis, MO), and examined with a Nikon Eclipse 90i microscope with a 100×/NA 1.4 phase-contrast oil immersion objective (Nikon, Melville, NY). Images were collected with an ORCA ER CCD camera (Hamamatsu, Bridgewater, NJ) and processed using Volocity (PerkinElmer, Waltham, MA).

For *O. lutea*, actively growing and motile cell filaments were collected, washed in ddH₂O, and left at 4 °C overnight to allow autolysis. For *Ph. autumnale*, actively growing and motile cell filaments were collected, washed in BG11 medium, and incubated at 50 °C for 14 hours. Subsequently, cells from both species were treated with 0.2 M Glycine buffer at pH 2.5 for 15 min at RT. After thorough washing in 20 mM HEPES at pH 8, cells were air-dried onto poly-L-lysine (PLL)-coated coverslips and submerged in 70% ethanol at −25 °C for 30 minutes for fixation. Coverslips were washed in PBS thoroughly and blocked in PBS containing 2% BSA and 0.5% Tween-20 at RT. Coverslips were placed cell-face down onto 100 µl drops of primary anti-PilQ at 1:600 dilutions in blocking buffer at RT. After one hour, coverslips were washed in blocking buffer, and further labeled with Alexa Fluor 488-conjugated secondary antibodies (Invitrogen, Carlsbad, CA) for

one hour at RT as above. After washing, coverslips were mounted with SlowFade Gold antifade mountant (Molecular Probes, Carlsbad, CA) and sealed with nail polish. Imaging was performed with a Nikon Eclipse Ti inverted fluorescence microscope using the Nikon Plan Apo 100× Ph oil (NA 1.45) objective (Nikon, Melville, NY). This was equipped with the Andor Zyla sCMOS camera (Andor, Belfast, NI). Image acquisition was controlled using NIS Elements AR 4.2 imaging software (Nikon Instruments, Netherlands). Images were visualized and analyzed with Fiji¹²¹.

Fluorescence imaging of EPS secretion

Actively motile *O. lutea* or *Ph. autumnale* cell filaments were collected and washed in BG11 media. The filaments were subjected to brief sonication (<1 second) at low power or cut into short fragments using sterile razor blades. Subsequently, the fragments were transferred to an ice-cold solution of BG11 containing 10 µg/ml of Alexa Fluor 488-conjugated concanavalin A (Invitrogen, Carlsbad, CA). Imaging was performed in a temperature regulated chamber set to 28 °C, using the same microscope for the IF imaging of *O. lutea* and *Ph. autumnale* described above. Cells were seeded into an ibidi PLL-treated µSlide V10.4 flow channel slide (ibidi, Gräfelfing, Germany) and allowed to settle for 5 minutes. BG11 was flowed through at >0.5 ml/s to remove excess concanavalin A and to encourage dissociation of slime bands from cell surfaces.

Serial dilution growth assay

To test the copper requirement for growth of the *M. xanthus* strains, cells were initially grown overnight in CTT media supplemented with 200 µM CuSO₄ at 32 °C. Subsequently, the cells were sub-cultured into CTT media devoid of copper but containing 200 µM of the copper chelator bathocuproinedisulfonic acid (BCS, Sigma-Aldrich, St. Louis, MO) and grown for 24 h at 32 °C. These cells were again sub-cultured into media with 200 µM BCS and grown for an additional 24 h at 32 °C. Cells were concentrated to 1 × 10⁹ cells/ml in CTT, and four 4-fold serial dilutions were prepared. Three microliters of each cell suspension were spotted on CTT plates with 1.5% agar, containing either 200 µM BCS, 100 µM CuSO₄, or 500 µM CuSO₄, dried, and incubated at 32 °C for 48 h.

Motility assays

For adventurous motility assays, mutant *M. xanthus* cells were grown overnight in liquid culture containing 200 µM CuSO₄ at 32 °C. Cells were then sub-cultured into media containing 200 µM BCS and grown for 24 h at 32 °C. Wildtype and *ΔpilA* cells were grown overnight in the absence of copper. Cells were diluted to 1 × 10⁸ cells/ml in CTT, and 10 µl were spotted onto 1/2× CTT plates with 1.5% agar, and either 200 µM BCS or 300 µM CuSO₄. Spots were dried and plates were incubated for 48 h at 32 °C. Swarm edges were examined with a Nikon Inverted TE200 microscope (Nikon, Melville, NY) using a 10× objective, and digital images were collected with a SPOT RT camera and SPOT Basic software (Diagnostic Instruments, Inc., Sterling Heights, MI).

Reporting summary

Further information on research design is available in the Nature Portfolio Reporting Summary linked to this article.

Data availability

The image reconstruction data have been deposited in the PDB database under accession code EMD-51272. Initial mass spectrometry identification of *A. platensis* PilQ (confirmed by two independent analyses) and the pentapeptide repeat protein NIES39_A07680 was performed at the Mass Spectrometry & Proteomics Resource Core, Harvard University, in 2011. Due to the significant amount of time that has passed since the original experiments, the raw instrument files required for PRIDE submission could not be obtained. However, the

original reports detailing these analyses are provided in Supplementary Data 1. All other data are available within the article and its Supplementary Information. Source data are provided with this paper. The mass spectrometry proteomics data have been deposited to the ProteomeXchange Consortium via the PRIDE partner repository with the dataset identifier PXD066729. Source data are provided with this paper.

References

- Costa, T. R. D. et al. Secretion systems in Gram-negative bacteria: structural and mechanistic insights. *Nat. Rev. Microbiol.* **13**, 343–359 (2015).
- Stoop, E. J., Bitter, W. & van der Sar, A. M. Tubercle bacilli rely on a type VII army for pathogenicity. *Trends Microbiol.* **20**, 477–484 (2012).
- McBride, M. J. & Zhu, Y. Gliding motility and Por secretion system genes are widespread among members of the phylum *Bacteroidetes*. *J. Bacteriol.* **195**, 270–278 (2013).
- Gorasia, D. G., Veith, P. D. & Reynolds, E. C. The type IX secretion system: advances in structure, function and organization. *Microorganisms* **8**, 1173 (2020).
- Grossman, A. S., Mauer, T. J., Forest, K. T. & Goodrich-Blair, H. A widespread bacterial secretion system with diverse substrates. *mBio* **12**, e0195621 (2021).
- Ilangovan, A., Connery, S. & Waksman, G. Structural biology of the Gram-negative bacterial conjugation systems. *Trends Microbiol.* **23**, 301–310 (2015).
- Whitney, J. C. & Howell, P. L. Synthase-dependent exopolysaccharides secretion in Gram-negative bacteria. *Trends Microbiol.* **21**, 63–72 (2013).
- Christie, P. J. The rich tapestry of protein translocation systems. *Protein J.* **38**, 389–408 (2019).
- Bayan, N., Guilvout, I. & Pugsley, A. P. Secretins take shape. *Mol. Microbiol.* **60**, 1–4 (2006).
- Korotkov, K. V., Gonen, T. & Hol, W. G. J. Secretins: dynamic channels for protein transport across membranes. *Trends Biochem. Sci.* **36**, 433–443 (2011).
- Tosi, T. et al. Structural similarity of secretins from type II and type III secretion systems. *Structure* **22**, 1348–1355 (2014).
- Opalka, N. et al. Structure of the filamentous phage IV multimer by cryo-electron microscopy. *J. Mol. Biol.* **325**, 461–470 (2003).
- Pelacic, V. Type IV pili: e pluribus unum?. *Mol. Microbiol.* **68**, 827–837 (2008).
- Korotkov, K. V., Sandkvist, M. & Hol, W. G. J. The type II secretion system: biogenesis, molecular architecture and mechanism. *Nat. Rev. Microbiol.* **10**, 336–351 (2012).
- Jain, S. et al. Structural characterization of outer membrane components of the type IV pili system in pathogenic *Neisseria*. *PLoS One* **6**, e16624 (2011).
- Thomas, S. R. & Trust, T. J. A specific PulD homolog is required for the secretion of paracrystalline surface array subunits in *Aeromonas hydrophila*. *J. Bacteriol.* **177**, 3932–3939 (1995).
- Abrusci, P., McDowell, M. A., Lea, S. M. & Johnson, S. Building a secreting nanomachine: a structural overview of the T3SS. *Curr. Opin. Struct. Biol.* **25**, 111–117 (2014).
- D’Imprima, E. et al. Cryo-EM structure of the bifunctional secretin complex of *Thermus thermophilus*. *eLife* **6**, e30483 (2017).
- Viarre, V. et al. HxcQ liposecretin is self-piloted to the outer membrane by its N-terminal lipid anchor. *J. Biol. Chem.* **284**, 33815–33823 (2009).
- Koo, J., Burrows, L. L. & Howell, L. Decoding the roles of pilotins and accessory proteins in secretin escort services. *FEMS Microbiol. Lett.* **328**, 1–12 (2012).
- Genin, S. & Boucher, C. A. A superfamily of proteins involved in different secretion pathways in Gram-negative bacteria: modular structure and specificity of the N-terminal domain. *Mol. Gen. Genet.* **243**, 112–118 (1994).
- Reichow, S. L., Korotkov, K. V., Hol, W. G. & Gonen, T. Structure of the cholera toxin secretion channel in its closed state. *Nat. Struct. Mol. Biol.* **17**, 1226–1232 (2010).
- Korotkov, K. V., Pardon, E., Streyaert, J. & Hol, W. G. J. Crystal structure of the N-terminal domain of the secretin GspD from ETEC determined with the assistance of a nanobody. *Structure* **17**, 255–265 (2009).
- Marlovits, T. C. et al. Structural insights into the assembly of the type III secretion needle complex. *Science* **306**, 1040–1042 (2004).
- Spagnuolo, J. et al. Identification of the gate regions in the primary structure of the secretin pIV. *Mol. Microbiol.* **76**, 133–150 (2010).
- Korotkov, K. V. & Sandkvist, M. Architecture, function, and substrates of the type II secretion system. *EcoSal* **8**, 10 (2019).
- Naskar, S., Hohl, M., Tassinari, M. & Low, H. H. The structure and mechanism of the bacterial type II secretion system. *Mol. Microbiol.* **115**, 412–424 (2021).
- Whitfield, C. Biosynthesis and assembly of capsular polysaccharides in *Escherichia coli*. *Annu. Rev. Biochem.* **75**, 39–68 (2006).
- Rehm, B. H. A. Bacterial polymers: biosynthesis, modifications and applications. *Nat. Rev. Microbiol.* **8**, 578–592 (2010).
- Whitfield, C., Wear, S. S. & Sande, C. Assembly of bacterial capsular polysaccharides and exopolysaccharides. *Annu. Rev. Microbiol.* **74**, 521–543 (2020).
- Toukach, P. V. & Egorova, K. S. Carbohydrate structure database merged from bacterial, archaeal, plant and fungal parts. *Nucl. Acids Res.* **44**, D1229–D1236.
- Skjåk-Bræk, G., Zanetti, F. & Paoletti, S. Effect of acetylation on some solution and gelling properties of alginates. *Carbohydr. Res.* **185**, 131–138 (1989).
- Franklin, M. J. et al. *Pseudomonas aeruginosa* AlgG is a polymer level alginate C5-mannuronan epimerase. *J. Bacteriol.* **176**, 1821–1830 (1994).
- Pérez-Burgos, M. & Søgaard-Andersen, L. Biosynthesis and function of cell-surface polysaccharides in the social bacterium *Myxococcus xanthus*. *Biol. Chem.* **401**, 1375–1387 (2020).
- Drummelsmith, J. & Whitfield, C. Translocation of group 1 capsular polysaccharide to the surface of *Escherichia coli* (O9a:K30) requires a multimeric complex in the outer membrane. *EMBO J.* **19**, 57–66 (2000).
- Liston, S. D., Mann, E. & Whitfield, C. Glycolipid substrates for ABC transporters required for the assembly of bacterial cell-envelope and cell-surface glycoconjugates. *Biochim. Biophys. Acta Mol. Cell Biol. Lipids* **1862**, 1394–1403 (2017).
- Paulsen, I. T., Beness, A. M. & Saier, M. H. J. Computer-based analyses of the protein constituents of transport systems catalyzing export of complex carbohydrates in bacteria. *Microbiology* **143**, 2685–2699 (1997).
- Cuthbertson, L., Mainprize, I. L., Naismith, J. H. & Whitfield, C. Pivotal roles of the outer membrane polysaccharide export and polysaccharide copolymerase protein families in export of exopolysaccharides in Gram-negative bacteria. *Microbiol. Mol. Biol. Rev.* **73**, 155–177 (2009).
- Morona, R., Purins, L., Tocilj, A., Matte, A. & Cygler, M. Sequence-structure relationships in polysaccharide co-polymerase (PCP) proteins. *Trends Biochem. Sci.* **34**, 78–84 (2009).
- Dong, C. et al. Wza, the translocon for *E. coli* capsular polysaccharides, defines a new class of membrane protein. *Nature* **444**, 226–229 (2006).
- Sathiyamoorthy, K., Mills, E., Franzmann, T. M., Rosenshine, I. & Saper, M. A. The crystal structure of *Escherichia coli* group 4

- capsule protein GfcC reveals a domain organization resembling that of Wza. *Biochemistry* **50**, 5465–5476 (2011).
42. Larson, M. R. et al. *Escherichia coli* O127 group 4 capsule proteins assemble at the outer membrane. *PLoS One* **16**, e0259900 (2021).
 43. Wiseman, B., Nitherwal, R. G., Widmalm, G. & Högbom, M. Structure of a full-length bacterial polysaccharide co-polymerase. *Nat. Commun.* **12**, 369 (2021).
 44. Yang, Y. et al. The molecular basis of regulation of bacterial capsule assembly by Wzc. *Nat. Commun.* **12**, 4349 (2021).
 45. Krasteva, P. V. et al. Insights into the structure and assembly of a bacterial cellulose secretion system. *Nat. Commun.* **8**, 2065 (2017).
 46. Hay, I. D., Wang, Y., Moradali, M. F., Rehman, Z. U. & Rehm, B. H. Genetics and regulation of bacterial alginate production. *Environ. Microbiol.* **16**, 2997–3011 (2014).
 47. Itoh, Y. et al. Roles of the *pgaABCD* genes in synthesis, modification, and export of the *Escherichia coli* biofilm adhesin poly- β -1,6-*N*-acetyl-D-glucosamine. *J. Bacteriol.* **190**, 3670–3680 (2008).
 48. Hubbard, C., McNamara, J. T., Azumaya, C., Patel, M. S. & Zimmer, J. The hyaluronan synthase catalyzes the synthesis and membrane translocation of hyaluronan. *J. Mol. Biol.* **418**, 21–31 (2012).
 49. Ross, P. et al. Regulation of cellulose synthesis in *Acetobacter xylinum* by cyclic diguanylic acid. *Nature* **325**, 279–281 (1987).
 50. Keiski, C. L. et al. AlgK is a TPR-containing protein and the periplasmic component of a novel exopolysaccharide secretin. *Structure* **18**, 265–273 (2010).
 51. Whitney, J. C. et al. Structural basis for alginate secretion across the bacterial outer membrane. *Proc. Natl. Acad. Sci. USA* **108**, 13083–13088 (2011).
 52. Reichenbach, H. & Dworkin, M. Introduction to the gliding bacteria. *The prokaryotes Vol. 1*, eds Starr, M. P., Stolp, H., Trüper, H. G., Balows, A. & Schlegel H. G. (Springer Press, Berlin, Heidelberg, New York) pp. 315–327 (1981).
 53. Hoiczky, E. & Baumeister, W. The junctional pore complex, a prokaryotic secretion organelle, is the molecular motor underlying gliding motility in cyanobacteria. *Curr. Biol.* **8**, 1161–1168 (1998).
 54. Wolgemuth, C., Hoiczky, E., Kaiser, D. & Oster, G. How myxobacteria glide. *Curr. Biol.* **12**, 369–377 (2002).
 55. Hoiczky, E. Structural and biochemical analysis of the sheath of *Phormidium uncinatum*. *J. Bacteriol.* **180**, 3923–3932 (1998).
 56. Ducret, A., Valignat, M. P., Mouhamar, F., Mignot, T. & Theodoly, O. Wet-surface-enhanced ellipsometric contrast microscopy identifies slime as a major adhesion factor during bacterial surface motility. *Proc. Natl. Acad. Sci. USA* **109**, 10036–10041 (2012).
 57. Lu, A. et al. Exopolysaccharide biosynthesis genes required for social motility in *Myxococcus xanthus*. *Mol. Microbiol.* **55**, 206–220 (2005).
 58. Nan, B. & Zusman, D. R. Uncovering the mystery of gliding motility in the myxobacteria. *Annu. Rev. Genet.* **45**, 21–39 (2011).
 59. Hoiczky, E. & Baumeister, W. Envelope structure of four gliding filamentous cyanobacteria. *J. Bacteriol.* **177**, 2387–2395 (1995).
 60. Hoiczky, E. Gliding motility in cyanobacteria: observations and possible explanations. *Arch. Microbiol.* **174**, 11–17 (2000).
 61. Nultsch, W. & Häder, D.-P. Über die Rolle der beiden Photosysteme in der Photophobotaxis von *Phormidium uncinatum*. *Ber. Dtsch. Bot. Ges.* **87**, 83–92 (1974).
 62. Belay, A. Mass culture of *Spirulina* outdoors - the Earthrise Farms experience. *Spirulina platensis (Arthrospira): physiology, cell-biology and biotechnology*, ed Vonshak A. (Francis & Taylor, London), pp. 131–158 (1997).
 63. Ohmori, K., Hirose, M. & Ohmori, M. Function of cAMP as mat-forming factor in the cyanobacterium *Spirulina platensis*. *Plant Cell Physiol.* **33**, 21–25 (1992).
 64. Walsby, A. E. Mucilage secretion and the movement of blue-green algae. *Protoplasma* **65**, 223–238 (1968).
 65. Black, K., Buikema, W. & Haselkorn, R. The *hglK* gene is required for localization of heterocyst-specific glycolipids in the cyanobacterium *Anabaena* sp. strain PCC7120. *J. Bacteriol.* **177**, 6440–6448 (1995).
 66. Varadi, M. et al. AlphaFold Protein Structure Database: massively expanding the structural coverage of protein-sequence space with high-accuracy models. *Nucleic Acids Res.* **50**, D439–D444 (2022).
 67. Jumper, J. et al. Highly accurate protein structure prediction with AlphaFold. *Nature* **596**, 583–589 (2023).
 68. Hoiczky, E. & Baumeister, W. Oscillin, an extracellular, Ca^{2+} -binding glycoprotein essential for the gliding motility of cyanobacteria. *Mol. Microbiol.* **26**, 699–708 (1997).
 69. Hoiczky, E. & Hansel, A. Cyanobacterial cell walls: news from an unusual prokaryotic envelope. *J. Bacteriol.* **182**, 1191–1199 (2000).
 70. Mehta, K. K., Evitt, N. H. & Swartz, J. R. Chemical lysis of cyanobacteria. *J. Biol. Eng.* **9**, 10 (2015).
 71. Kaiser, D. Social gliding is correlated with the presence of pili in *Myxococcus xanthus*. *Proc. Natl. Acad. Sci. USA* **76**, 5952–5956 (1979).
 72. Wall, D., Kohlenbrandner, P. E. & Kaiser, D. The *Myxococcus xanthus pilQ* (*sglA*) gene encodes a secretin homolog required for type IV pilus biogenesis, social motility, and development. *J. Bacteriol.* **181**, 24–33 (1999).
 73. Chang, Y.-W. et al. Architecture of the type IVa pilus machine. *Science* **351**, aad2001 (2016).
 74. Zuckerman, D. M., Hicks, S. W., Charron, G., Hang, H. C. & Machamer, C. E. Differential regulation of two palmitoylation sites in the cytoplasmic tail of the beta1-adrenergic receptor. *J. Biol. Chem.* **286**, 19014–19023 (2011).
 75. Gómez-Santos, N. et al. Comprehensive set of integrative plasmid vectors for copper-inducible gene expression in *Myxococcus xanthus*. *Appl. Environ. Microbiol.* **78**, 2515–2521 (2012).
 76. Koch, M., McHugh, C. A. & Hoiczky, E. BacM, an N-terminally processed bactofilin of *Myxococcus xanthus*, is crucial for cell shape. *Mol. Microbiol.* **80**, 1031–1051 (2011).
 77. Yu, R. & Kaiser, D. Gliding motility and polarized slime secretion. *Mol. Microbiol.* **63**, 454–467 (2007).
 78. Fluegel, W. Simple method for demonstrating myxobacterial slime. *J. Bacteriol.* **85**, 1173–1174 (1963).
 79. Pelling, A. E., Li, Y., Shi, W. & Gimzewski, J. K. Nanoscale visualization and characterization of *Myxococcus xanthus* cells with atomic force microscopy. *Proc. Natl. Acad. Sci. USA* **102**, 6484–6489 (2005).
 80. Dworkin, M. Fibrils as extracellular appendages of bacteria: their role in contact-mediated cell-cell interactions in *Myxococcus xanthus*. *Bioessays* **21**, 590–595 (1999).
 81. Palsdottir, H. et al. Three-dimensional macromolecular organization of cryofixed *Myxococcus xanthus* biofilms as revealed by electron microscopic tomography. *J. Bacteriol.* **191**, 2077–2082 (2009).
 82. Remis, J. P. et al. Bacterial social networks: structure and composition of *Myxococcus xanthus* outer membrane vesicle chains. *Environ. Microbiol.* **16**, 598–610 (2013).
 83. Holkenbrink, C., Hoiczky, E., Kahnt, J. & Higgs, P. I. Synthesis and assembly of a novel glycan layer in *Myxococcus xanthus* spores. *J. Biol. Chem.* **289**, 32364–32378 (2014).
 84. Islam, S. T. et al. Modulation of bacterial multicellularity via spatio-specific polysaccharide secretion. *PLoS Biol.* **18**, e3000728 (2020).
 85. Nan, B., McBride, M. J., Chen, J., Zusman, D. R. & Oster, G. Bacteria that glide with helical tracks. *Curr. Biol.* **24**, R169–R173 (2014).
 86. Hartzell, P. L., Shi, W. & Youderian, P. Gliding motility of *Myxococcus xanthus*. *Myxobacteria: multicellularity and*

- differentiation, ed Whitworth, D. E. (ASM Press, Washington DC), pp. 103–122 (2008).
87. Costerton, J. W., Geesey, G. G. & Cheng, K. J. How bacteria stick. *Sci. Am.* **238**, 86–95 (1978).
 88. Costerton, J. W., Stewart, P. S. & Greenberg, E. P. Bacterial biofilms: a common cause of persistent infections. *Science* **284**, 1318–1322 (1999).
 89. Flemming, H. C. & Wingender, J. The biofilm matrix. *Nat. Rev. Microbiol.* **8**, 623–633 (2010).
 90. Otto, M. Physical stress and bacterial colonization. *FEMS Microbiol. Rev.* **38**, 1250–1270 (2014).
 91. Hall-Stoodley, L., Costerton, J. W. & Stoodley, P. Bacterial biofilms: from the natural environment to infectious diseases. *Nat. Rev. Microbiol.* **2**, 95–108 (2004).
 92. Stewart, P. S. & Franklin, M. J. Physiological heterogeneity in biofilms. *Nat. Rev. Microbiol.* **6**, 199–210 (2008).
 93. Danhorn, T. & Fuqua, C. Biofilm formation by plant-associated bacteria. *Annu. Rev. Microbiol.* **61**, 401–422 (2007).
 94. Lebeaux, D., Ghigo, J. M. & Beloin, C. Biofilm-related infections: bridging the gap between clinical management and fundamental aspects of recalcitrant towards antibiotics. *Microbiol. Mol. Biol. Rev.* **78**, 510–543 (2014).
 95. Berleman, J. E. & Kirby, J. R. Deciphering the hunting strategy of a bacterial wolfpack. *FEMS Microbiol. Rev.* **33**, 942–957 (2009).
 96. Velicer, G. J. & Vos, M. Sociobiology of the myxobacteria. *Annu. Rev. Microbiol.* **63**, 599–623 (2009).
 97. Konovalova, A., Petters, T. & Sogaard-Andersen, L. Extracellular biology of *Myxococcus xanthus*. *FEMS Microbiol. Rev.* **34**, 89–106 (2010).
 98. Kahnt, J. et al. Profiling the outer membrane proteome during growth and development of the social bacterium *Myxococcus xanthus* by selective biotinylation and analysis of outer membrane vesicles. *J. Proteome Res.* **9**, 5197–5208 (2010).
 99. Pan, H.-W. et al. Seawater-regulated genes for two-components systems and outer membrane proteins in *Myxococcus*. *J. Bacteriol.* **191**, 2102–2111 (2009).
 100. Bateman, A., Murzin, A. G. & Teichmann, S. A. Structure and distribution of pentapeptide repeats in bacteria. *Protein Sci.* **7**, 1477–1480 (1998).
 101. Andrade, M. A., Perez-Iratxeta, C. & Pointing, C. P. Protein repeats: structures, functions, and evolution. *J. Struct. Biol.* **134**, 117–131 (2001).
 102. Sah, G. P., Cao, P. & Wall, D. MYXO-CTERM sorting tag directs proteins to the cell surface via the type II secretion system. *Mol. Microbiol.* **113**, 1038–1051 (2020).
 103. Pathak, D. T. et al. Cell contact-dependent outer membrane exchange in myxobacteria: genetic determinants and mechanism. *PLoS Genet.* **8**, e1002626 (2012).
 104. Zhang, C. Y. et al. New locus important for *Myxococcus* social motility and development. *J. Bacteriol.* **189**, 7937–7941 (2007).
 105. Watson, B. F. & Dworkin, M. Comparative intermediary metabolism of vegetative cells and microcysts of *Myxococcus xanthus*. *J. Bacteriol.* **96**, 1465–1473 (1968).
 106. Risser, D. D. & Meeks, J. C. Comparative transcriptomics with a motility-deficient mutant leads to identification of a novel polysaccharide secretion system in *Nostoc punctiforme*. *Mol. Microbiol.* **87**, 884–893 (2013).
 107. Disconzi, E. et al. Bacterial secretins form constitutively open pores akin to general porins. *J. Bacteriol.* **196**, 121–128 (2014).
 108. Khayatan, B., Meeks, J. C. & Risser, D. D. Evidence that a modified type IV pilus-like system powers gliding motility and polysaccharide secretion in filamentous cyanobacteria. *Mol. Microbiol.* **98**, 1021–1036 (2015).
 109. Guglielmi, G. & Cohen-Bazire, G. Comparative study of the structure and distribution of extracellular filaments (fimbriae) in some cyanobacteria. *Protistologica* **18**, 167–177 (1982).
 110. Halfen, L. N. & Castenholz, R. W. Gliding in a blue-green alga: a possible mechanism. *Nature* **225**, 1163–1165 (1970).
 111. Farag, A. T. An integrated approach for landfill leachate treatment using plasma/UV pretreatment and indigenous green microalgae. PhD Thesis, University of Sheffield (2022).
 112. Wu, S. S. & Kaiser, D. Markerless deletions of *pil* genes in *Myxococcus xanthus* generated by counterselection with the *Bacillus subtilis* *sacB* gene. *J. Bacteriol.* **178**, 5817–5821 (1996).
 113. Ueki, T., Inouye, S. & Inouye, M. Positive-negative KG cassettes for construction of multi-gene deletions using a single drug marker. *Gene* **183**, 153–157 (1996).
 114. Lee, B., Schramm, A., Jagadeesan, S. & Higgs, P. I. Two-component systems and regulation of developmental progression in *Myxococcus xanthus*. *Methods Enzymol.* **471**, 253–278 (2010).
 115. Cox, J. & Mann, M. MaxQuant enables high peptide identification rates, individualized p.p.b.-range mass accuracies and proteome-wide protein quantification. *Nat. Biotechnol.* **26**, 1367–1372 (2008).
 116. Reynolds, E. S. The use of lead citrate at high pH as an electron-opaque stain for electron microscopy. *J. Cell Biol.* **17**, 208–212 (1963).
 117. Hrabe, T. et al. PyTom: A python-based toolbox for localization of macromolecules in cryo-electron tomograms and subtomogram analysis. *J. Struct. Biol.* **178**, 177–188 (2012).
 118. Nickel, S. et al. TOM software toolbox: Acquisition and analysis for electron tomography. *J. Struct. Biol.* **149**, 227–234 (2005).
 119. Punjani, A., Rubinstein, J. L., Fleet, D. J. & Brubaker, M. A. cryoSPARC: algorithms for rapid unsupervised cryo-EM structure determination. *Nat. Methods* **14**, 290–296 (2017).
 120. Pettersen, E. F. et al. UCSF ChimeraX: Structure visualization for researchers, educators, and developers. *Protein Sci.* **30**, 70–82 (2021).
 121. Schindelin, J. et al. Fiji: an open-source platform for biological-image analysis. *Nat. Methods* **9**, 676–682 (2012).

Acknowledgements

We thank Colleen McHugh and Harriet Pratley for the generation of GspD/PilQ antisera, José Muñoz-Dorado for providing plasmids for copper-inducible gene expression, Tâm Mignot, Emilia Mauriello, and Penelope Higgs for providing carbohydrate deletion strains, Daniel Bollschweiler, Florian Beck, and Harald Engelhardt (MPI of Biochemistry, Martinsried) for their help with averaging the negatively stained *A. platensis* PilQ complexes (Fig. S7), Christopher Hill and Svet Tzokov for help with the high-pressure freezing and cryo-electron microscopy, and Carolyn Machamer for providing research space for D.M.Z. Mass spectrometry analyses were carried out by Trong Khoa Pham at the biOMICS/chemMS Facility of the Faculty of Science Mass Spectrometry Center at the University of Sheffield, by William S. Lane at the Mass Spectrometry & Proteomics Resource Core at Harvard University, and by Ulf Bergmann at Proteome Factory AG in Berlin, Germany. Light microscopy was performed at the Wolfson Light Microscopy Facility. This research was funded in part by a National Institutes of Health General Medicine Grant (GM85024 to E.H.), a Forschungssstipendium of the Max Planck Society (to E.H.), a BBSRC CBMNet Proof-of-Concept Award (to E.H.), a National Institutes of Health Infectious Disease and Immunology Training Grant (to D.M.Z.), and a National Science Foundation Grant (1949762 to D.M.Z.). In addition, E.H., J.M.T.S., and D.M.Z. acknowledge support from the Imagine: Imaging Life initiative of the University of Sheffield.

Author contributions

E.H. performed thin-sectioning, staining, and imaging of samples, biochemical purification of nozzle-like structures, M.S. identification of the protein(s), and performed motility assays in cyanobacteria. J.S. performed cryo-EM image acquisition and reconstruction, IFM to visualize

PilQ localization and slime secretion in cyanobacteria, and sequence analysis. E.H. and D.Z. visualized outer membranes for nozzle-like structures via EM and performed the single-cell slime-secretion assays. D.Z. affinity-purified the anti-GspD antibody, generated the *gspD* conditional knockdown mutant of *M. xanthus*, and performed immunoblot, IFM, culture, and gliding motility assays. All authors contributed to experimental design, data interpretation, and writing the manuscript.

Competing interests

The authors declare no competing interests.

Additional information

Supplementary information The online version contains supplementary material available at <https://doi.org/10.1038/s41467-025-63426-x>.

Correspondence and requests for materials should be addressed to Egbert Hoiczyk.

Peer review information *Nature Communications* thanks Beiyan Nan and the other anonymous reviewers for their contribution to the peer review of this work.

Reprints and permissions information is available at <http://www.nature.com/reprints>

Publisher's note Springer Nature remains neutral with regard to jurisdictional claims in published maps and institutional affiliations.

Open Access This article is licensed under a Creative Commons Attribution-NonCommercial-NoDerivatives 4.0 International License, which permits any non-commercial use, sharing, distribution and reproduction in any medium or format, as long as you give appropriate credit to the original author(s) and the source, provide a link to the Creative Commons licence, and indicate if you modified the licensed material. You do not have permission under this licence to share adapted material derived from this article or parts of it. The images or other third party material in this article are included in the article's Creative Commons licence, unless indicated otherwise in a credit line to the material. If material is not included in the article's Creative Commons licence and your intended use is not permitted by statutory regulation or exceeds the permitted use, you will need to obtain permission directly from the copyright holder. To view a copy of this licence, visit <http://creativecommons.org/licenses/by-nc-nd/4.0/>.

© The Author(s) 2025